Volume 7, Issue 12 – January – June – 2020

ECORFAN

Journal-Bolivia

ISSN-On line: 2410-4191

ECORFAN®

ECORFAN Journal-Bolivia, Volume 7 Number 12, June - 2020, is a biannual Journal edited by ECORFAN-Bolivia and the international academy. Santa Lucia N-21, Barrio Libertadores, Cd. Sucre. Chuquisaca, Bolivia, http://www.ecorfan.org/bolivia/journal.php, journal@ecorfan.org. Editor in charge: Fernando Iglesias-Suarez, MsC ISSN: 2410-4191. Responsible for the last update of this issue ECORFAN Computer Unit. Imelda Escamilla Bouchán, PhD. Vladimir Luna Soto, PhD. Santa Lucia N-21, Barrio Libertadores, Cd. Sucre. Chuquisaca, Bolivia. Date of last update June 30, 2020.

ECORFAN-Journal Bolivia

Definition of the Journal

Scientific Objectives

Support the international scientific community in its written production Science, Technology and Innovation in the Field of Medicine and Health Sciences, in Subdisciplines Engineering, Chemical, Optical, Resources, Food technology, Anatomy, Nutrition.

ECORFAN-Mexico S.C. is a Scientific and Technological Company in contribution to the Human Resource training focused on the continuity in the critical analysis of International Research and is attached to CONACYT-RENIECYT number 1702902, its commitment is to disseminate research and contributions of the International Scientific Community, academic institutions, agencies and entities of the public and private sectors and contribute to the linking of researchers who carry out scientific activities, technological developments and training of specialized human resources with governments, companies and social organizations.

Encourage the interlocution of the International Scientific Community with other Study Centers in Mexico and abroad and promote a wide incorporation of academics, specialists and researchers to the publication in Science Structures of Autonomous Universities - State Public Universities - Federal IES - Polytechnic Universities - Technological Universities - Federal Technological Institutes - Normal Schools - Decentralized Technological Institutes - Intercultural Universities - S & T Councils - CONACYT Research Centers.

Scope, Coverage and Audience

ECORFAN -Journal Bolivia is a Journal edited by ECORFAN-Mexico S.C in its Holding with repository in Bolivia, is a scientific publication arbitrated and indexed with semester periods. It supports a wide range of contents that are evaluated by academic peers by the Double-Blind method, around subjects related to the theory and practice of Engineering, Chemical, Optical, Resources, Food technology, Anatomy, Nutrition with diverse approaches and perspectives , That contribute to the diffusion of the development of Science Technology and Innovation that allow the arguments related to the decision making and influence in the formulation of international policies in the Field of Medicine and Health Sciences. The editorial horizon of ECORFAN-Mexico® extends beyond the academy and integrates other segments of research and analysis outside the scope, as long as they meet the requirements of rigorous argumentative and scientific, as well as addressing issues of general and current interest of the International Scientific Society.

Editorial Board

Arbitration Committee

Assignment of Rights

The sending of an Article to ECORFAN -Journal Bolivia emanates the commitment of the author not to submit it simultaneously to the consideration of other series publications for it must complement the Originality Format for its Article.

The authors sign the Authorization Format for their Article to be disseminated by means that ECORFAN-Mexico, S.C. In its Holding Bolivia considers pertinent for disclosure and diffusion of its Article its Rights of Work.

Declaration of Authorship

Indicate the Name of Author and Coauthors at most in the participation of the Article and indicate in extensive the Institutional Affiliation indicating the Department.

Identify the Name of Author and Coauthors at most with the CVU Scholarship Number-PNPC or SNI-CONACYT- Indicating the Researcher Level and their Google Scholar Profile to verify their Citation Level and H index.

Identify the Name of Author and Coauthors at most in the Science and Technology Profiles widely accepted by the International Scientific Community ORC ID - Researcher ID Thomson - arXiv Author ID - PubMed Author ID - Open ID respectively.

Indicate the contact for correspondence to the Author (Mail and Telephone) and indicate the Researcher who contributes as the first Author of the Article.

Plagiarism Detection

All Articles will be tested by plagiarism software PLAGSCAN if a plagiarism level is detected Positive will not be sent to arbitration and will be rescinded of the reception of the Article notifying the Authors responsible, claiming that academic plagiarism is criminalized in the Penal Code.

Arbitration Process

All Articles will be evaluated by academic peers by the Double Blind method, the Arbitration Approval is a requirement for the Editorial Board to make a final decision that will be final in all cases. MARVID® is a derivative brand of ECORFAN® specialized in providing the expert evaluators all of them with Doctorate degree and distinction of International Researchers in the respective Councils of Science and Technology the counterpart of CONACYT for the chapters of America-Europe-Asia- Africa and Oceania. The identification of the authorship should only appear on a first removable page, in order to ensure that the Arbitration process is anonymous and covers the following stages: Identification of the Journal with its author occupation rate - Identification of Authors and Coauthors - Detection of plagiarism PLAGSCAN - Review of Formats of Authorization and Originality-Allocation to the Editorial Board-Allocation of the pair of Expert Arbitrators-Notification of Arbitration -Declaration of observations to the Author-Verification of Article Modified for Editing-Publication.

Instructions for Scientific, Technological and Innovation Publication

Knowledge Area

The works must be unpublished and refer to topics of Engineering, Chemical, Optical, Resources, Food technology, Anatomy, Nutrition and other topics related to Medicine and Health Sciences.

Presentation of the Content

In the first chapter we present, *Emotion classification from EEG signals using wearable sensors: pilot test*, by JARILLO-SILVA, Alejandro, GOMEZ-PEREZ, Víctor A., ESCOTTO-CÓRDOVA, Eduardo A. and DOMÍNGUEZ-RAMÍREZ, Omar A., with ascription in the Universidad de la Sierra Sur, Universidad Autónoma del Estado de Hidalgo and Universidad Nacional Autónoma de México, as a second article we present, *Noise analysis using Tucker decomposition and PCA on spectral images*, by PADILLA-ZEPEDA, Efraín, TORRES-ROMAN, Deni and MENDEZ-VAZQUEZ, Andrés, with secondment in the Instituto Politécnico Nacional, as the following article we present, *Synthesis and incorporation of ZnO/TiO_2 in PMMA to study its thermal propertiese*, by GAYTÁN-LARA, Francisco Javier, ZÁRRAGA–NUÑEZ Ramón and GALINDO-GONZÁLEZ, Rosario, with affiliation at the Universidad de Guanajuato, as next article we present, *Magnetite coupling in a PS/PMMA block copolymer using suspension polymerization*, by CARMONA-TORRES Marco, FUENTES-RAMÍREZ, Rosalba, CONTRERAS-LOPEZ David and GALINDO-GONZÁLEZ, Rosario, with affiliation at the Universidad de Guanajuato.

Content

Article **ECORFAN Journal-Bolivia**
June 2020 Vol.7 No.12 1-9

Emotion classification from EEG signals using wearable sensors: pilot test

Clasificación de las emociones a partir de las señales de EEG con sensores portátiles: prueba piloto

JARILLO-SILVA, Alejandro†*´, GOMEZ-PEREZ, Víctor A.´, ESCOTTO-CÓRDOVA, Eduardo A.´´ and DOMÍNGUEZ-RAMÍREZ, Omar A.´´´

´Universidad de la Sierra Sur, Instituto de Informática, Centro de Tecnologías de la Información, Laboratorio de Interacción Humano Computadora
´´Universidad Autónoma del Estado de Hidalgo, Research Center on Information and Systems Technology, Electronics and Control Group
´´´Universidad Nacional Autónoma de México, Facultad de Estudios Superiores Zaragoza, Carrera de Psicología, Av. Guelatao No. 66, Col. Ejército de Oriente, alcaldía de Iztapalapa, CDMX

ID 1st Author: *Alejandro, Jarillo-Silva* / **ORC ID:** 0000-0002-9776-6533, **CVU CONACYT ID:** 241966

ID 1st Coauthor: *Víctor A., Gómez-Pérez* / **ORC ID:** 0000-0002-7758-6690, **CVU CONACYT ID:** 222462

ID 2nd Coauthor: *Eduardo A. Escotto-Córdova* / **ORC ID:** 0000-0002-1104-8195, **CVU CONACYT ID:** 168236

ID 3rd Coauthor: *Omar A., Domínguez Ramírez* / **ORC ID:** 0000-0002-9663-8089, **CVU CONACYT ID:** 202942

DOI: 10.35429/EJB.2020.12.7.1.9 Received January 19, 2020; Accepted June 29, 2020

Abstract

The objective of this work is to present a procedure for the classification of basic emotions based on the analysis of EEG signals (electroencephalogram). For this case, 25 subjects were stimulated, of whom 17 were men and 9 women between 20 and 35 years of age. The stimulus to induce positive, negative and neutral emotions with a certain level of excitation (activation) was a set of video clips previously evaluated. The processed and analyzed signals belong to the gamma and beta frequency bands of the F3, F4, P7, P8, T7, T8, O1 and O2 electrodes. The characteristic variables with the best result are the entropy of each band of each electrode. The cross validation algorithms are applied and later the main component analysis algorithm. Finally, four classifier algorithms are used: classifier trees, Support- Vector-Machine (SVM), Linear-Discriminant-Analysis (LDA) and k-Nearest-Neighbors (KNN). The results confirm that by carrying out the proposed procedure, the EEG signals contain enough information to allow the recognition of basic emotions.

EEG signal analysis (Electroencephalogram), Machine learning, Recognition of Emotions

Resumen

El objetivo de este trabajo es presentar un procedimiento para la clasificación de emociones básicas basado en el análisis de señales de EEG (electroencefalograma). Para este caso, se estimularon 25 sujetos, de los cuales 17 fueron hombres y 9 mujeres entre 20 y 35 años de edad. El estímulo para inducir emociones positivas, negativas y neutras con un cierto nivel de excitación (activación) fue un conjunto de videoclips evaluados previamente. Las señales procesadas y analizadas pertenecen a las bandas de frecuencia gamma y beta de los electrodos F3, F4, P7, P8, T7, T8, O1 y O2. Las variables características con mejor resultado son la entropía de cada banda en cada electrodo. Se aplican los algoritmos de validación cruzada y posteriormente el algoritmo de análisis de principales componentes. Finalmente, se emplean cuatro algoritmos clasificadores: árboles clasificadores, SupportVector-Machine (SVM), Linear-Discriminant- Analysis (LDA) y k-Nearest-Neighbours (KNN). Los resultados confirman que llevando acabo el procedimiento planteado, las señales de EEG contienen suficiente información para permitir el reconocimiento de las emociones básicas.

Análisis de señales EEG (Electroencefalograma), Aprendizaje automático, Reconocimiento de emociones

Citation: JARILLO-SILVA, Alejandro, GOMEZ-PEREZ, Víctor A., ESCOTTO-CÓRDOVA, Eduardo A. and DOMÍNGUEZ-RAMÍREZ, Omar A. Emotion classification from EEG signals using wearable sensors: pilot test. ECORFAN Journal-Bolivia. 2020. 7-12: 1-9.

* Correspondence to Author (E-mail: ajarillo0205@gmail.com)
† Researcher contributing first author.

Introduction

In recent years, the volume of studies and publications on the recognition of emotions has increased. Thanks to technological advancement, techniques and models have been diversified in the generation of systems for the detection of emotions. These systems can be easily differentiated between them; for example, the use of various stimuli, the characteristics for the classification, the size of the time window, the classifiers, the number of participants and the models of emotions. Most research related to emotion detection is mainly based on the biosignal treaty. These can be obtained from different devices, such as; an electroencephalograph (ECG), an electroencephalogram (EEG), galvanic-sensor-response (GSR), thermal imaging cameras, etc (Koelstra et al., 2011) and in (Li & Lu, 2009). Thanks to access to technology in recent years the amount of research has increased significantly, where they make use of an EEG (electroencephalograph), however, the field of research is still very wide.

The effectiveness and efficiency of algorithms for the biosignals treaty still show limitations. According to Herger (2013) these include response time, precision, number of electrodes, number of recognized emotions, and the generation of a robust control group database.

The expression of emotions, not only facially, but bodily, mainly involves the bioelectrical activity of various brain structures: the cingulum, the nucleus accumbens, the insula, the orbitofrontal and medial zone, the hypothalamus, the pituitary, the hippocampus, and the amygdala among the most prominent. Unfortunately, with electrodes placed on the scalp that record brain signals (EEG), it is not possible to distinguish or record the relative participation of each one, nor its dynamic participation in each of the possible emotions. However, the signals that are recorded and amplified with an EEG can be correlated with the induction of emotions, especially if a general classification of emotions is used, that is, positive or negative. During the presence of emotions, changes in the electrical signals of the brain are manifested, which are related to the voltage levels (result of ionic current flows within the neurons in the brain) and frequency.

The electrical activity of the brain is classified according to the high and low frequency rhythms called frequency bands. These bands have been defined through studies of psychological and physiological phenomena associated with brain activity.

According to Megías (2011) the study of emotions under experimental conditions has become a fundamental tool to understand the psychological and neurobiological processes involved in their development. Over the last decades, various strategies have been successfully used to induce emotions in experimental conditions (e.g., images, music, videos, self-induction, etc.). Currently the use of scenes from movies (vide films) to induce emotions is one of the most widely used techniques, since it has important advantages such as greater ecological validity since they are stimuli more similar to those perceived in real life. In addition, they are dynamic and different perceptual channels intervene (visual and auditory), allow the standardization and reproduction of the procedure, and allow the induction of specific basic emotions.

In this work, we present a procedure that controls the stimulation of emotions from an intra-subject experimental design, the processing of EEG signals and the evaluation of classification algorithms.

The rest of this document is organized as follows. In Section II a review of the literature is made, describing the models of emotion, stimuli, characteristics, time window and classifier. Section III presents the methodology used in this research. Section IV presents the results obtained. Section V presents a discussion of the results obtained. Finally, Section VI describes the conclusions reached in this work.

Literature review

The factors that have determined different results in different investigations using an EEG are: emotion model, stimulus, characteristic, time window and the classifier. These factors are described below.

ISSN-On line: 2410-4191

JARILLO-SILVA, Alejandro, GOMEZ-PEREZ, Víctor A., ESCOTTO-CÓRDOVA, Eduardo A. and DOMÍNGUEZ-RAMÍREZ, Omar A. Emotion classification from EEG signals using wearable sensors: pilot test. ECORFAN Journal-Bolivia. 2020

Models of emotion

Emotions according to the literature can be classified based on two models: categorical or discrete and dimensional (Bradley & Lang,1994) and in (Gray, 2011). The dimensional model proposes that emotional states can be accurately represented by a small number of underlying affective dimensions. That is, it represents the continuous emotional state as a vector in a multidimensional space. Most dimensional models incorporate valence and activation. Valence refers to the degree of "liking" associated with an emotion. It ranges from unpleasant (eg, sad, stressed) to pleasant (eg, happy, exalted). Whereas, activation refers to the force of the emotion experienced. This activation occurs along a continuum and can range from inactive (eg, uninteresting, boring) to active (eg, alert, excited) (Posner, Russell & Peterson, 2011). This model is used in many investigations for its ease of expressing an emotion in terms of valence and arousal (see Figure 1)

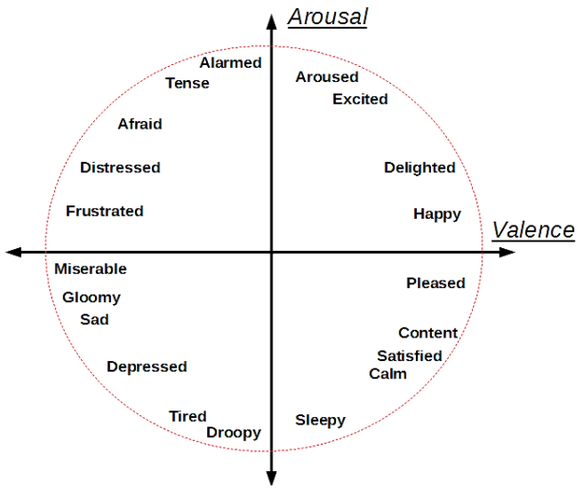

Figure 1 Dimensional model of emotion
Source: (Russell, 1980)

Discrete theories of emotion propose the existence of small amounts of separate emotions. These are characterized by coordinated response patterns in physiology, neural anatomy, and morphological expressions. According to Herger (2013) six basic emotions frequently used in research papers include happiness, sadness, anger, disgust, fear, and surprise

Stimuli

It is defined as the way or way to evoke or induce a certain emotion. Some researchers claim that video clips are the best stimuli, while others find that music or even memories is better. What is clear is that a robust and strong stimulator causes performance with good results, since it guarantees the induction of a certain emotion. Some types of stimulation are: images (Neath-Tavares & Itier, 2016), video clips (Daşdemir, Yıldırım & Yıldırım, 2017), music (Daly et al., 2015), memories (Chanel et al., 2015), self-induction (Iacoviello et al., 2015), games (Chanel et al, 2011), etc. There are generalized databases for the stimulation of emotions, for example, the IAPS (International Affective Picture Systmes), the IADS (International Digitized Sound System) and the GADEP (Geneva Affcetive Picture Database). These databases are the result of the average emotional evaluations of a group of many people.

On the other hand, there are published databases of physiological information collected during the stimulation of a certain emotion. DEAP (Dataset for Emotion Analysis using Physiological) which includes data collected from 32 subjects (17 men with an average age of 27.2 $\pm$ 4.4 years) and SEED (SJTU EEG database) which contains the collection of 62 channels from 15 subjects (7 men of 23.7 $\pm$ 2.37 years), where the subjects were stimulated with 15 videos of 4 minutes each. The induced emotions were positive, neutral and negative.

However, if analyzes of the DEAP and SEED databases are performed, non-conclusive results are obtained, such is the case of the comparison made by Li et al. (2018) where using SEEE an accuracy of 59.06% and DEAP of 83% are obtained. It is one of the reasons why this research does not make use of these databases. In Mexico there are various indigenous languages and cultural traditions that influence their categorization, expression and perception. For this reason, the stimulus used is based on video clips, previously validated by the study community.

ISSN-On line: 2410-4191

Features

There are a considerable number of variables extracted from EEG signals to be considered representative characteristics of the electrical activity of the brain. In the frequency domain the most widely used is PSD (Power Spectral Density), the power of the EEG signal in its frequency bands using Fourier transform (Al-Nafjan et al., 2017). In the time domain they are: activity, mobility and complexity, using the Hjorth parameters and the Fractal dimension with the Higuchi method (Yuvaraj & Murugappan, 2016). In the Wavelet domain: entropy and energy using Wavelet transform (Zhang, et al, 2015). Statistical characteristics: mean, standard deviation, Kurtosis, Skewness, etc (Friedrich et al., 2015).

However, it is interesting to note that nonlinearity in the brain is introduced even at the cellular level, since the dynamic behavior of individual neurons is governed by threshold and saturation phenomena. In this way, on a global level, the brain also presents a really complex and heterogeneous performance, which means that its behavior is far from being considered linear. This research makes use of characteristics based on the study of "log-energy" entropy, which in the described context are justified.

Temporary window

The appropriate length of the time window largely depends on the type of emotion and physiological signal used. According to Jatupaiboon, Pan-ngum & Israsena (2013) on average the emotion time is between 0.5 and 4 seconds. When using an inappropriate window, the emotion may be misclassified because different emotions may be present when the periods are too long. Existing literature does not provide an adequate window size to achieve optimal EEG-based emotion recognition. A window size of 1 second is used in this investigation.

Algorithm classifier

A number of machine learning algorithms have been employed for the classification of emotions, such as SVM (Support Vector Machine), K-NN (K- Nearest Neighbors), LDA (Linear Discriminant Analysis), NM (Naiver Bayes), trees classifiers, ANN (Artificial Neuronal Network), etc.

However, in this research a comparison is developed between K-NN, SVM and classifier trees using the "log-energy" entropy as a characteristic.

Methodology

The hypothesis that "induced emotions are correlated with electroencephalographic patterns" has been tried with different emotional induction procedures. However, there are different variables, both of the recording of signals (noise, artifacts, etc.) and of the stimuli used in the induction of emotions (images of faces) as characteristics of the participants (race, age, sex, language, culture, etc.) that influence the results. This results in difficulty in inducing a real emotional response using generalized artificial techniques. On the other hand, if a controlled experiment is guaranteed under the same operating conditions, where in addition, the selection of participants meet inclusion criteria, then it is possible to induce an emotional response with the appropriate stimulus.

Based on the above, this section describes the development of two models to predict: one the level of emotion in the dimensions of affective valence (positive, neutral or negative) and the second model the level of activation (high, neutral or low). Figure 2 shows the architecture, which is made up of four main modules: stimulation of the subject, acquisition and processing of the data, extraction of the characteristics and evaluation of the performance of the models.

ISSN-On line: 2410-4191

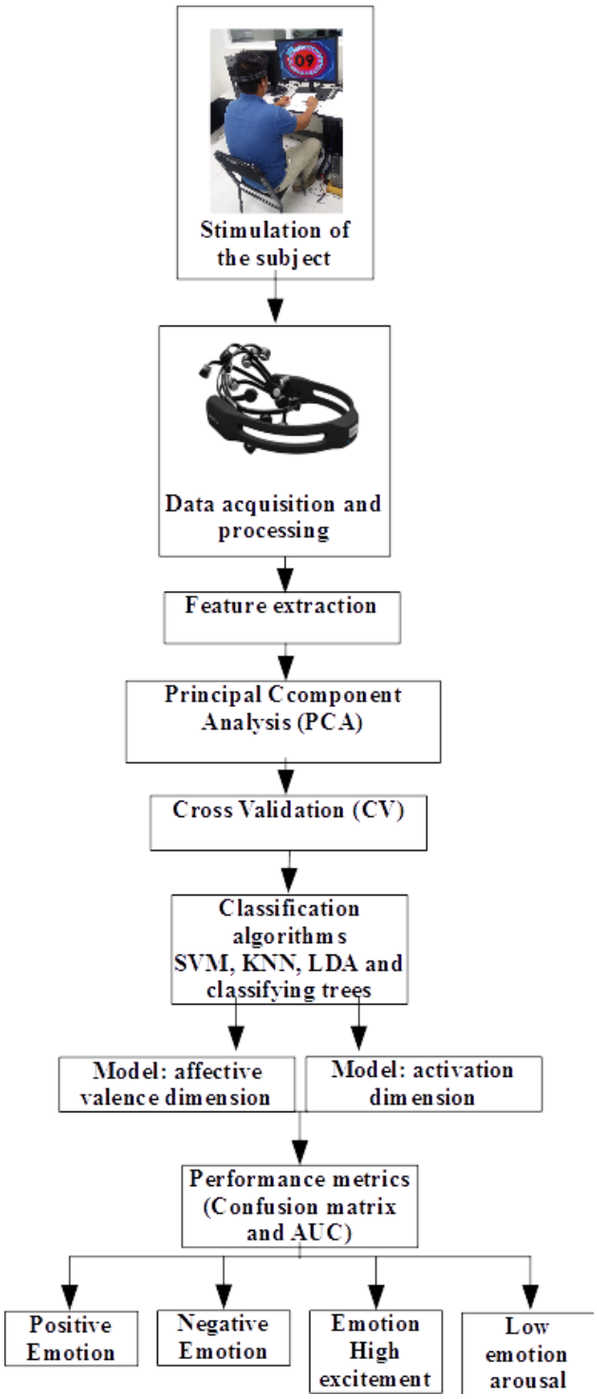

Figure 2 General model architecture

Stimuli

The experiment involved 25 healthy subjects between 18 and 35 years with an average of 23.7 years, 17 male and 9 female, from the Sierra Sur region of Oaxaca, which were selected for convenience. Exclusion criteria are based on whether the subject is at neurological or psychiatric risk and addictions to alcohol or drugs.

In order to stimulate different emotions in the study subjects, seven validated video clips were used. Each video stimulates a particular emotion with greater intensity. Subjects evaluate each of the videos in terms of valence and excitement using the Self-Assessment Mannequin (SAM) instrument. In these tests, the liker scale is used to quantify arousal and pleasure. They are represented by graphic images that express 9 levels (Morris, 1995).

Figure 3 shows the process for the induction of emotions, which is based on a cross-case study. It begins with the recording of signals from a baseline, in this case the subject remains seated with his eyes open facing a black screen for 35 seconds. Subsequently, the subject is stimulated by a video with a duration of between 3 and 5 minutes. At the end of each video clip you must answer the SAM (Select Assessment for Manufacturing) test, which allows you to know subjectively the assessment of each video in two dimensions (see Figure 4).

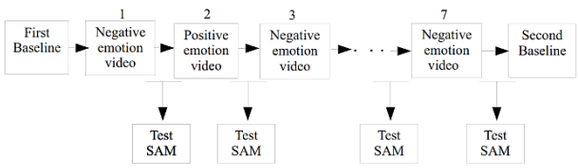

Figure 3 Emotion induction process

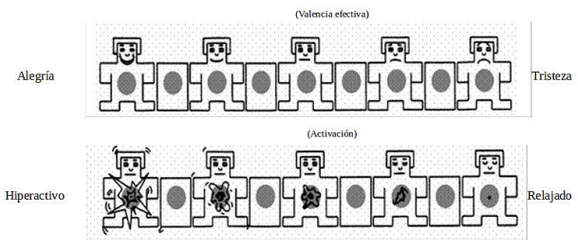

Figure 4 Sam test for two dimensions

After 30 seconds of having finished the first video, the subject is stimulated again with another video, at the end, the subject answers the SAM test corresponding to the immediately previous video, this is repeated until the subject has seen all the videos continuously. At the end of the videos, a second baseline is obtained, which is analyzed and stored in the data processing. The experiment lasts approximately 28.5 minutes.

ISSN-On line: 2410-4191

Data acquisition and processing

For this research, the EMOTIV EPOC device is used, which consists of 14 channels (AF3, AF4, FC6, FC5, F3, F4, P7, P8, T7, T8, O1 and O2) located according to the international system 10 -20. Each electrode provides a sampling rate of 128 Hz and a resolution of 14 bits (see Figure 5. The data is sent to the computer wirelessly using Bluetooth technology. Emotiv Pro software provides raw data for each of the channels, which is stored in a file with the * csv extension.

Emotiv Epoc device complies with many regulatory requirements like Federal communication commission (FCC) rules part 15, Radio standard specification (RSS) 210 and low voltage requirement rule: Directive 2006/95/EC. FCC ensures that the device may not cause any harmful interference and the interference received should not cause any undesired operation. RSS-210 is to ensure that the device itself should not cause any interference. (Emotiv, 2016a.)

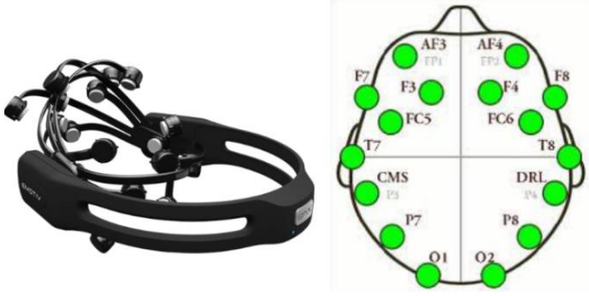

Figure 5 Emotiv device and electrode position system 10-20 modified

To manipulate the information extracted from the device, a data grouping method was developed. This method allows organizing and filtering the relevant information, reducing the dimensionality of the data set, in order to search for characteristics that best define the emotional state. This methodology optimized the training and prediction process of the models.

Feature extraction

Alpha, beta and gamma signals are of great interest in emotion research. However, the presence of noise from artifacts such as eyepieces (below 4 Hz), heart sounds (around 1.2 Hz) and muscle (above 30 Hz) are eliminated by using only the bands of beta and gamma frequency.

On the other hand, nonlinear analysis has proven to be valuable in the evaluation of physiological time series, since hidden information related to the mechanisms has been obtained in a wide variety of clinical settings. However, although there are a large number of nonlinear measurements, entropies based on quantification of the regularity of time series have been widely used in recent years, as they can work as a success even on short and noisy recordings (Pincus, 1991).

Performance evaluation of classifying algorithms

From the extracted characteristics, the next step is to compare the performance of the classifying algorithms proposed in this investigation. Classifying algorithms are used to provide two models. The valence dimension model has three classes: positive, negative, and neutral. The arousal model consists of three classes; high, low and neutral. In each model, the sensitivity, specificity and percentage of accuracy are obtained. From the Area Under Curve (AUC) it is determined if the model is appropriate to identify emotions.

To avoid overfitting the data when generating each model, it is used k-fold cross-validation (k-fold CV). This algorithm randomly divides the information into k-1 subsets where 80% of the data is destined to train and build the model, while 20% of the remaining data was reserved to evaluate and validate the classifier. The objective of cross-validation is to ensure independence between partitions of training and test data. In this procedure k = 5 were used.

On the other hand, the PCA (Principal Component Analysis) algorithm is used. The objective is that from a set of observations of possibly correlated variables they are converted into a set of linearly uncorrelated variables. In this case of a total of 24 variables, 7 linearly uncorrelated variables were found.

Results

To analyze the results of the SVM, K-NN, LDA and classifier trees algorithms, the confusion matrix was implemented, which contains information about the actual and predicted classification of each algorithm. Table 1 shows the performance of each classifying algorithm in each model.

ISSN-On line: 2410-4191

Classifier Algorithms	Valence	Arousal
Classifying trees	74.3%	60.8%
SVM	83.2%	78.8%
KNN	**83.7%**	**81.1%**
LDA	67.3%	47%

Table 1 Accuracy results of each classifier algorithm with the respective model

Performance evaluation of the KNN classifier algorithm

The classifier algorithm with the best performance in this pilot test is KNN. The KNN algorithm in the affective valence dimension presents a true positive rate of 85% and a false negative rate of 15% to identify a negative class. While for the neutral class 15% of the data identifies it as positive and 14% as negative (see Table 2). Furthermore, the area under the AUC curve = 0.94, which is interpreted as the appropriate KNN algorithm to identify positive, negative and neutral emotions. This means that this classifying algorithm has a better chance of discerning between positive, negative and neutral emotions.

True classes	-	-	-	-	-
Negative	85%	12%	2%	85%	15%
Positive	15%	83%	2%	83%	17%
Neutral	14%	15%	71%	71%	29%
Predicted classes	*Negative*	*Positive*	*Neutral*	*True positive*	*False negative*

Table 2 Confusion matrix of the KNN algorithm for the affective valence dimension

The Table 3 shows the confusion matrix for the arousal dimension. The KNN classifier algorithm presents a prediction accuracy for a high emotion of 82%, while to predict if the emotion is low level it is 79%. On the other hand, of all the data that correspond to the neutral class, only 18% incorrectly predict it. The results of the confusion matrix analysis indicate that it has a true positive prediction rate of 82%. While the false positive rate is 13%. The AUC is 0.93, which indicates that the algorithm is discriminant to define if there is a high arousal level, a very low level or a neutral level.

True classes	-	-	-	-	-
Low	**79%**	19%	2%	79%	21%
High	16%	**82%**	2%	82%	18%
Neutral	8%	9%	**82%**	72%	28%
Predicted classes	*Low*	*High*	*Neutral*	*True high*	*False low*

Table 3 Confusion matrix of the KNN algorithm for the arousal dimension

Finally, Table IV presents the results of the SAM test evaluation. It is observed that video clips 1, 3, 5 and 7 induce a very low level in the valence dimension, which is interpreted as very negative emotion. Videos 2, 4 and 6 induce a very positive emotion. In the arousal dimension, videos 5 and 7 indicate a high level of excitement while videos 1, 2, 3, 4 and 6 induce a low level of excitation.

Videos	Stimulation	Valence	Arousal
1	Negative	1.8	3.0
2	Positive	6.7	2.7
3	Negative	3.2	2.8
4	Positive	6.1	2.7
5	Negative	1.5	4.8
6	Positive	6.7	2.1
7	Negative	1.9	6.4

Table 4 SAM test results

Discussions

In this work, we verify the effectiveness of a procedure considering a cross-case study for the induction and recognition of basic emotions. Where entropy is considered as a unique characteristic of the beta frequency bands and range of an EEG. Furthermore, the process allows comparing the performance of classifying algorithms using EEG signals to predict basic emotions.

The results show that the EEG signals contain enough information to distinguish between high, low and neutral in the arousal dimension. While for the valence dimension, distinguish between positive and negative and neutral in affective valence. Furthermore, in particular the KNN classifier algorithm using entropy as its only characteristic is able to distinguish between these classes, although it is worth noting that the SVM model gives results very similar to the KNN.

Subjects play an important role in evaluating classifiers. An attempt was made to select the subjects adequately, so that based on the exclusion criteria, there were no biases in the results. However, although there is an initial baseline, there was no evaluation at the beginning of the experiment that allowed determining the emotional state of the subject. Incorporating information from the subject's emotional state at the start of the experiment probably improves the results of the classifying algorithms.

ISSN-On line: 2410-4191

The results in Table 4 show that the video clips induce the expected emotion, both in the affective and activation valence dimensions.

This correlates with the results of the KNN classifier model. On the other hand, although tests were made using the 14 electrodes of the Emotiv device, the F3, F4, P7, P8, T7, T8, O1 and O2 electrodes were the ones that provide the greatest variability information in emotion detection.

Conclusions

In this work we have explored the way to distinguish positive and negative emotions, as well as to discern between emotions with a high activation level (excitation) and with a low level.

The use of databases to stimulate emotions does not guarantee favorable results, since it has been seen that much depends on the cultural, social and sometimes even political aspects. According to the results of the pilot test, the use of exclusive videos to stimulate basic emotions in the Oaxaca region of Mexico presents optimistic results.

The use of classifying algorithms in the study of emotions based on EEG information is a way that guarantees encouraging results. Among the algorithms most used for this type of procedure, the KNN provides efficiency and effectiveness in recognizing basic emotions.

However, the cross-validation and PCA algorithms are important to achieve that the classifier algorithm provides favorable results in terms of its sensitivity and specificity.

Finally, it is not necessary to use all the electrodes of the Emotiv device for the study of emotions, with only 8 favorable results were obtained.

In future work, it is intended to use only one pair of electrodes, which will generate sufficient evidence to identify emotions in the affective and arousal valence dimensions.

Acknowledgments

This research work was supported by PRODEP, IDCA 21306, code UNSIS-CA-13 in the 2018 Strengthening of Academic Bodies call.

References

Al-Nafjan, A., Hosny, M., Al-Wabil, A., & Al-Ohali, Y. (2017). Classification of human emotions from electroencephalogram (EEG) signal using deep neural network. International Journal of Advanced Computer Science and Applications, 8(9), 419-425.

Bradley, M. M., & Lang, P. J. (1994). Measuring emotion: the self-assessment manikin and the semantic differential. Journal of behavior therapy and experimental psychiatry, 25(1), 49-59.

Chanel, G., Kierkels, J. J., Soleymani, M., & Pun, T. (2009). Short-term emotion assessment in a recall paradigm. International Journal of Human-Computer Studies, 67(8), 607-627.

Chanel, G., Rebetez, C., Bétrancourt, M., & Pun, T. (2011). Emotion assessment from physiological signals for adaptation of game difficulty. IEEE Transactions on Systems, Man, and Cybernetics-Part A: Systems and Humans, 41(6), 1052-1063.

Daly, I., Williams, D., Hallowell, J., Hwang, F., Kirke, A., Malik, A & Nasuto, S. J. (2015). Music-induced emotions can be predicted from a combination of brain activity and acoustic features. Brain and cognition, 101, 1-11.

Daşdemir, Y., Yıldırım, E., & Yıldırım, S. (2017). Emotion Analysis using Different Stimuli with EEG Signals in Emotional Space. Natural and Engineering Sciences, 2(2), 1-10.

Emotiv. (2016). Epoc -14 Channel Wireless EEG Headset Description. https://www.emotiv.com/epoc/.

Friedrich, E. V., Sivanathan, A., Lim, T., Suttie, N., Louchart, S., Pillen, S., & Pineda, J. A. (2015). An effective neurofeedback intervention to improve social interactions in children with autism spectrum disorder. Journal of autism and developmental disorders, 45(12), 4084-4100.

Gray, J. R. (2001). Emotional modulation of cognitive control: Approach–withdrawal states double-dissociate spatial from verbal two-back task performance. Journal of Experimental Psychology: General, 130(3), 436.

ISSN-On line: 2410-4191

Heger, D., Mutter, R., Herff, C., Putze, F., & Schultz, T. (2013). Continuous recognition of affective states by functional near infrared spectroscopy signals. In 2013 Humaine Association Conference on Affective Computing and Intelligent Interaction (pp. 832-837). IEEE.

Iacoviello, D., Petracca, A., Spezialetti, M., & Placidi, G. (2015). A real-time classification algorithm for EEG-based BCI driven by self-induced emotions. Computer methods and programs in biomedicine, 122(3), 293-303.

Jatupaiboon, N., Pan-ngum, S., & Israsena, P. (2013). Emotion classification using minimal EEG channels and frequency bands. In The 2013 10th International Joint Conference on Computer Science and Software Engineering (JCSSE) (pp. 21-24). IEEE.

Koelstra, S., Muhl, C., Soleymani, M., Lee, J. S., Yazdani, A., Ebrahimi, T., & Patras, I. (2011). Deap: A database for emotion analysis; using physiological signals. IEEE transactions on affective computing, 3(1), 18-31.

Li, X., Song, D., Zhang, P., Zhang, Y., Hou, Y., & Hu, B. (2018). Exploring EEG features in cross-subject emotion recognition. Frontiers in neuroscience, 12, 162.

Li, M., & Lu, B. L. (2009). Emotion classification based on gamma-band EEG. In 2009 Annual International Conference of the IEEE Engineering in medicine and biology society (pp. 1223-1226). IEEE.

Megías, C. F., Mateos, J. C. P., Ribaudi, J. S., & Fernández-Abascal, E. G. (2011). Validación española de una batería de películas para inducir emociones. Psicothema, 23(4), 778-785.

Morris, J. D. (1995). Observations: SAM: the Self-Assessment Manikin; an efficient cross-cultural measurement of emotional response. Journal of advertising research, 35(6), 63-68.

Neath-Tavares, K. N., & Itier, R. J. (2016). Neural processing of fearful and happy facial expressions during emotion-relevant and emotion-irrelevant tasks: a fixation-to-feature approach. Biological psychology, 119, 122-140.

Pincus, S. M. (1991). Approximate entropy as a measure of system complexity. Proceedings of the National Academy of Sciences, 88(6), 2297-2301.

Posner, J., Russell, J. A., & Peterson, B. S. (2005). The circumplex model of affect: An integrative approach to affective neuroscience, cognitive development, and psychopathology. Development and psychopathology, 17(3), 715-734.

Yuvaraj, R., & Murugappan, M. (2016). Hemispheric asymmetry non-linear analysis of EEG during emotional responses from idiopathic Parkinson's disease patients. Cognitive neurodynamics, 10(3), 225-234.

Zhang, C., Tong, L., Zeng, Y., Jiang, J., Bu, H., Yan, B., & Li, J. (2015). Automatic artifact removal from electroencephalogram data based on a priori artifact information. BioMed research international, 2015.

ISSN-On line: 2410-4191

Article **ECORFAN Journal-Bolivia**
June 2020 Vol.7 No.12 10-16

Noise analysis using Tucker decomposition and PCA on spectral images

Análisis de ruido utilizando descomposición de Tucker y PCA en imágenes espectrales

PADILLA-ZEPEDA, Efraín†*, TORRES-ROMAN, Deni and MENDEZ-VAZQUEZ, Andrés

Instituto Politécnico Nacional, Center for Research and Advanced Studies, Telecommunications Group.

ID 1st Author: *Efraín, Padilla-Zepeda* / **ORC ID:** 0000-0002-9880-7157, **CVU CONACYT ID**: 924485

ID 1st Coauthor: *Deni, Torres-Román* / **ORC ID:** 0000-0002-9813-7712, **CVU CONACYT ID**: 20075

ID 2nd Coauthor: *Andrés, Méndez-Vázquez* / **CVU CONACYT ID**: 52042

DOI: 10.35429/EJB.2020.12.7.10.16 Received: January 15, 2020; Accepted: June 30, 2020

Abstract

Given the improvement of Remote Sensing (RS) sensors, it has been possible to increase spatial and spectral resolution on many of them. Nevertheless, the amount of data to represent and post-process has become highly prohibitive. Therefore, the need to be able to process such huge data sets, and one of the possible ways to deal with problems is the use of compression methods, however, data loss happen if the need of data size reduction is a must. RS spectral imagery contain high quantities of redundant information along the spectral domain, thus, making possible to use compression methods effectively as for example, tensor decomposition algorithms. In Tucker decomposition (TKD), an interesting and strange phenomenon happens when spatial domain is maintained and spectral domain is reduced, as a preprocessing step of a semantic segmentation task. Under these conditions, it is possible to observe an improvement on Pixel Accuracy (PA) metric when it is compared with the same uncompressed spectral image. Therefore, this work presents a study on how noise affects the Tucker Decomposition compared with Principal Component Analysis (PCA) and its impact in semantic segmentation.

Spectral Image, Tucker Decomposition, Noise

Resumen

Dada la mejora de los sensores de percepción remota, ha sido posible aumentar la resolución espacial y espectral en muchos de ellos. Sin embargo, la cantidad de datos para representar y postprocesar se ha vuelto altamente prohibitiva. Por lo tanto, existe la necesidad de poder procesar grandes conjuntos de datos, y una de las formas posibles de lidiar con este problema es el uso de métodos de compresión, sin embargo, la pérdida de datos es inevitable. Las imágenes espectrales contienen gran cantidad de información redundante a lo largo del dominio espectral, por lo tanto, es posible utilizar métodos de compresión de manera efectiva como, por ejemplo, algoritmos de descomposición tensorial. En la descomposición de Tucker, ocurre un fenómeno interesante y extraño cuando se mantiene el dominio espacial y se reduce el dominio espectral, como una etapa de preprocesamiento de segmentación semántica. Bajo estas condiciones, es posible observar una mejora en la precisión de píxeles cuando se compara con la misma imagen espectral sin comprimir. Por lo tanto, este trabajo presenta un estudio sobre cómo el ruido afecta la descomposición de Tucker en comparación con el análisis de componentes principales y su impacto en segmentación semántica.

Imagen spectral, Descomposición de Tucker, Ruido

Citation: PADILLA-ZEPEDA, Efraín, TORRES-ROMAN, Deni and MENDEZ-VAZQUEZ, Andrés. Noise analysis using Tucker decomposition and PCA on spectral images. ECORFAN Journal-Bolivia. 2020. 7-13:10-16.

* Correspondence to Author (Email: asanchezv@ipn.mx)
† Researcher contributing as first author

Introduction

The Greek word "spectral", which relates to "colors", combined with "image" figuratively mean "image of colors". This concept is based on taking a portion of the electromagnetic spectrum and breaking it into pieces for the purpose of analytical computations (Borengasser *et al*., 2007). Therefore, in this paper, we took the decision to represent the Spectral Images (SI) as tensors given their flexibility as data representation. Why to take such choice? On possible answer is that spectral images images contain abundant spatial and spectral information and is always corrupted by various noises, especially Gaussian Noise (Kong *et al*., 2019), making necessary to look for good representations of such spatial data and noise. Not only that, there is a generalized problem in spectral imagery applications with noise, given that, the performace is highly dependent on the Signal to Noise Ratio (SNR) (Rasti *et al*., 2018).

A strange phenomenon happen on spectral imagery when spatial domain is maintained and spectral domain is reduced through Tucker decomposition as a preprocessing step of a semantic segmentation task, seen in (López *et al*., 2020), since we can observe an improvement on Pixel Accuracy (PA) metric compared with uncompressed spectral image.

In this work, we have done a noise analysis after two compression methods which are Principal Component Analysis (PCA) and Tucker Decomposition (TKD). In such methods, it has been possible to observe some bands of the resulting images after compression and compare it graphically. Also, compare the PA in Semantic Segmentation task through a Neural Network (Multi-Layer Perceptron) in both cases.

This work is organized as follows: Section 2 introduces basic concepts of tensors and notation. Section 3 presents some concepts of the noise present in spectral imagery. In section 4 the theory behind compression methods that are implemented in this work are defined. In section 5 the experiments and results are presented. Finally, in section 6 the results are discussed.

Tensor Algebra Notation and Spectral Image Representation

A tensor is a multidimensional array. The order of a tensor is the number of its dimensions, also called the ways or modes. Therefore and Nth-order is an array with N dimensions (Kolda & Bader, 2009).

The following notation is used in this paper:

x : a scalar.

$\mathbf{x}$: a 1st-order tensor or a vector.

$\mathbf{X}$: a 2nd-order tensor or a matrix.

$\boldsymbol{\mathcal{X}}$: a 3rd-order tensor.

$x_{i,j,\ldots,n}$: the element $(i,j,\ldots,n)$ of a tensor $\boldsymbol{\mathcal{X}}$.

$\mathbf{x}_i$: the ith column of a matrix $\mathbf{X}$.

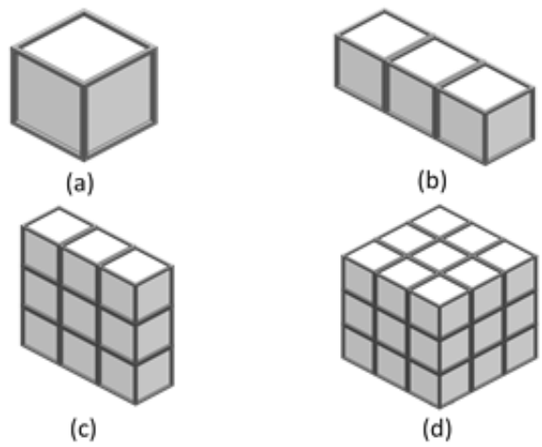

Figure 1 Graphic tensor examples. (a) $x \in \mathbb{R}$: a scalar, (b) $\mathbf{x} \in \mathbb{R}^{\mathbf{3}}$: a 1st-order tensor, (c) $\mathbf{X} \in \mathbb{R}^{\mathbf{3\times3}}$: a 2nd-order tensor, (d) $\boldsymbol{\mathcal{X}} \in \mathbb{R}^{\mathbf{3\times3\times3}}$: a 3rd-order tensor
Source: own work [SolidWorks].

Thus, the representation of a SI is a 3rd-order tensor:

$\boldsymbol{\mathcal{S}}$: Spectral image (1)

Where $\boldsymbol{\mathcal{S}} \in \mathbb{R}^{h\times w\times b}$, h, w and b are the number of elements (pixels) in Mode-1 (column), Mode-2 (row) and Mode-3 (tube) fibers respectively

ISSN-On line: 2410-4191

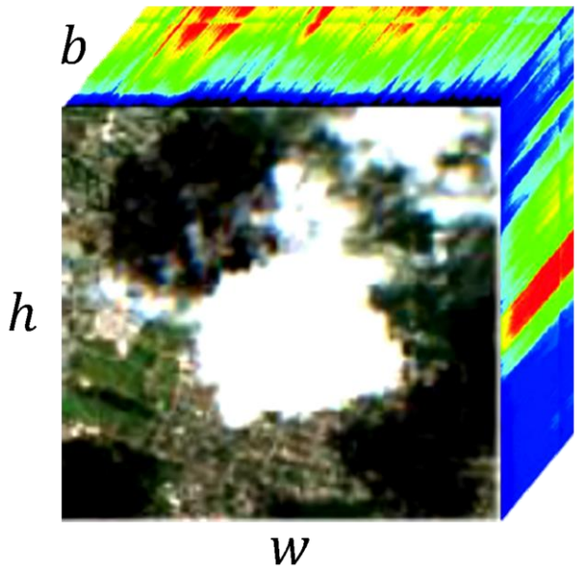

Figure 2 Spectral image example, where h, w and b are the height (rows), width (columns) and bands (tubes) respectively
Source: Sentinel-2 mission. ESA

Noise Assumptions

The presence of different noise sources in a SI makes its modelling and the denoising task very challenging, therefore, SI denoising approaches often consider either of the following types or a mixture of them as seen in (Rasti *et al*., 2018):

Noise Types

Signal Independent Noise

Thermal noise and quantization noise in HSI are modeled by signal independent Gaussian additive noise. Usually, noise is assumed to be uncorrelated spectrally having a diagonal noise covariance matrix, the model was introduced by (Landgrebe & Makaret, 1986).

The Gaussian assumption has been broadly used in hyperspectral analysis since it considerably simplifies the analysis and the noise variance estimation.

Sparse Noise

Impulse noises such as salt and pepper noise, missing pixels, missing lines and other outliers often exist in the acquired SI and are usually due to a malfunctioning of the sensor.

Pattern Noise

Spectral imaging systems may also induce artifacts in spectral images, usually referred to as pattern noise.

Additive Noise and Simulated Noise Generation

Generally, in the state of the art can be found many ways to get (Rasti *et al*., 2018):

$$\boldsymbol{\mathcal{S}} = \boldsymbol{\mathcal{X}} + \boldsymbol{\mathcal{N}} \tag{2}$$

Where $\boldsymbol{\mathcal{S}}, \boldsymbol{\mathcal{X}}, \boldsymbol{\mathcal{N}} \in \mathbb{R}^{h \times w \times b}$ are the noisy SI, clean SI and the additive noise of the SI respectively.

There are many other noises (i.e. multiplicative noise), nevertheless, for this work we are going to consider only the additive noise for its simplicity and good results in noise modeling.

The noise can be generated by adding zero-mean Gaussian noise as seen in (Rasti *et al*., 2018)(Bioucas-Dias & Nascimento, 2008).

$$N = [n_{ij}] \tag{3}$$

Where $n_{ij} \sim N(0, \sigma_i^2)$ is normally distributed.
The variance of the noise σ_i^2 variates along the spectral axis according to:

$$\sigma_i^2 = \sigma^2 \frac{e^{-\frac{(i-p/2)^2}{2\eta^2}}}{\sum_{j=1}^{p} e^{-\frac{(j-p/2)^2}{2\eta^2}}} \tag{4}$$

Where the power of the noise is controlled by σ, and η behaves like the standard deviation of a Gaussian bell curve, p is the number of bands. In this work, we consider only the additive noise as expressed by equation (2), the noise is generated with variances given by equation (4) (Landgrebe & Makaret, 1986).

ISSN-On line: 2410-4191

Compression Methods

Principal Component Analysis (PCA)

Large datasets are increasingly common and are often difficult to interpret. PCA is a technique for reducing the dimensionality of such datasets, increasing interpretability but at the same time minimizing information loss. It does by creating new uncorrelated variables that successively maximize variance. Finding such new variable, the principal components, reduces to solving an eigenvalue/eigenvector problem. For further information see (Jollife & Cadima, 2016).

For a given standardized dataset $\mathbf{A} \in \mathbb{R}^{m \times n}$ we get the covariance matrix from

$$\mathbf{C} = \mathbf{A}^{T}\mathbf{A} \tag{5}$$

Where $\mathbf{C} \in \mathbb{R}^{n \times n}$.

The n eigenvectors obtained from $\mathbf{C}$ are the principal components of the dataset and its corresponding eigenvalues are related with its importance. Discarding some of the less significant components (the number of components discarded depends of the application) we can get a transformation matrix $\mathbf{X}$ with the k remaining components in its columns, the dimensions of $\mathbf{X}$ are n by k.

From the following equation we get the new compressed dataset $\mathbf{Y}$ from the linear transformation of the original standardized dataset $\mathbf{A}$ multiplied by the transformation matrix $\mathbf{X}$.

$$\mathbf{Y} = \mathbf{AX} \tag{6}$$

Where $\mathbf{Y} \in \mathbb{R}^{m \times k}$.

To apply PCA and compress along the spectral domain of a SI, we get the vectorized frontal slices (h by w) of $\boldsymbol{\mathcal{S}}$. These vectors will be the columns of $\mathbf{A}$, thus $\mathbf{A} \in \mathbb{R}^{hw \times b}$ is a matricized form of $\boldsymbol{\mathcal{S}}$.

Tucker Decomposition (TDK)

Is a form of higher-order PCA. It decomposes a tensor into a core tensor multiplied (or transformed) by a matrix along each mode. Thus, in the three-way case where $\boldsymbol{\mathcal{X}} \in \mathbb{R}^{I \times J \times K}$ we have

$$\boldsymbol{\mathcal{X}} \approx \boldsymbol{\mathcal{G}} \times_1 \mathbf{A} \times_2 \mathbf{B} \times_3 \mathbf{C} \tag{7}$$

The tensor $\boldsymbol{\mathcal{G}}$ is called the core tensor, and $\mathbf{A}$, $\mathbf{B}$ and $\mathbf{C}$ are the factor matrices and can be thought of as the principal components in each mode. In order to compress only along the last mode (in depth of the cube), we exchange the factor matrices with identity matrices.

$$\boldsymbol{\mathcal{X}} \approx \boldsymbol{\mathcal{G}} \times_1 \mathbf{I} \times_2 \mathbf{I} \times_3 \mathbf{C} \tag{8}$$

The core tensor keeps the first two dimensions (spatial) but depth dimension (spectral) is reduced. There are many algorithms to compute the TKD like High Order Singular Value Decomposition (HOSVD) or Alternating Least Squares (ALS), for further information see (Kolda & Bader, 2009).

Dataset and Experiments

Dataset Description

The dataset consist of 115 scenes, each scene contain a multi-spectral image with dimensions $128 \times 128 \times 9$, an RGB reference image with dimensions $128 \times 128 \times 3$ and a corresponding matrix of labels with dimensions 128×128 from the Sentinel-2 mission of the of the European Space Agency (ESA) on Central Europe. Each pixel is labeled with one of the following classes of interest: Soil, shadow, cloud, vegetation or water.

Experiments

Experiment 1 – Band-1 Visualization after PCA and TKD Compression

In this experiment we took the 50th scene (out of 115) of the study case dataset with dimensions ($128 \times 128 \times 9$). We added simulated noise to the spectral image and after this, perform PCA and the TKD compressing the spectral domain. In the scene we observe a small vegetation zone at the top, a city in the middle and a mass of water in the RGB reference image, also we visualize only the first band (out of 9) of the study scene represented in grayscale in Fig. 3.

ISSN-On line: 2410-4191

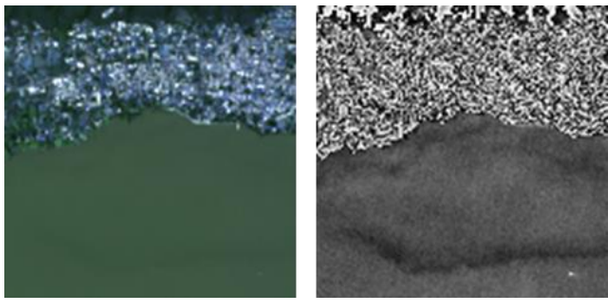

Figure 3 RGB reference image (left) and band-1 (right)
Source: ESA, own work [Python 3.7.6]

We have added simulated noise as seen in section 3.2 with parameters $\sigma = 13$ and $\eta = 72$ selected based on graphic empirical results.

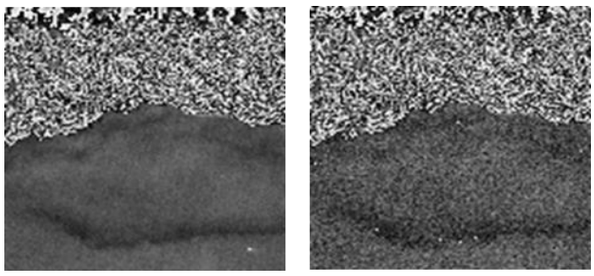

Figure 4 Band-1 of the study scene. Comparison between original (left) and added simulated noise (right).
Source: own work [Python 3.7.6]

After performed a spectral compression of the study scene with added simulated noise through PCA to 3 components and TDK to 3 tensorial bands preserving the spatial domain. An important remark is that we have done a reconstruction from the compressed study scene in both cases (from 3 components/tensorial bands back to the original 9 bands) only for visualization purposes in Fig. 5.

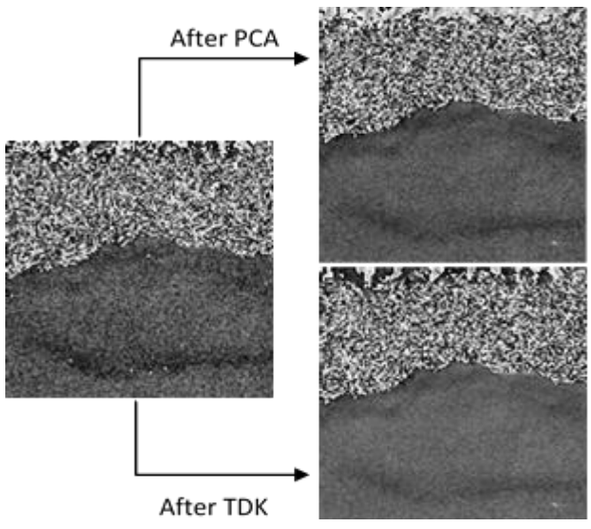

Figure 5 Band-1 of the study scene with added simulated noise (left), reconstruction of band-1 after PCA (top-right), reconstruction of band-1 after TKD (bottom-right)
Source: own work [Python 3.7.6]

Is easy to see a noise reduction over the mass of water zone in both cases, also we can observe a better performance of TKD over the vegetation zone.

Experiment 2 – Semantic Segmentation

In this section we reproduce the phenomenon of pixel accuracy improvement at some amount of the compression of multi-spectral images seen in (López et al., 2020) with the compression as a preprocessing step of a supervised pixel-wise semantic segmentation task.

Spectral image compression is performed in all possible cases from 9 original bands to (8, 7, …, 1) Principal Components (PC) in the case of PCA and compressed to (8, 7, …, 1) Tensorial Bands (TB) in the case of TKD. As a reminder, the images are only compressed in the spectral domain, spatial domain is kept for pixel-wise classification purposes.

The 115 compressed SI in tensor form was matricized into $\mathbf{X}$ such that each pixel is in each row and its corresponding values along the spectral axis are in the columns. The dimensions of the matrix $\mathbf{X}$ to be used in the classifications task are 115×128×128 by "b" bands, b depends of the amount of compression done by PCA or TKD, thus $\mathbf{X} \in \mathbb{R}^{\mathbf{1,884,160} \times b}$. The labels are vectorized into $\mathbf{y}$ in the same way to preserve the spatial relation. $\mathbf{X}$ and $\mathbf{y}$ was splitted picking random samples into .7-train/.3-test partition. RGB reference images are not used in this experiment.

For pixel-wise supervised classification of the 115 scenes we used a generic Multi-Layer Perceptron (MLP) neural network with the following parameters:

Parameter:	Value:
Number of hidden layers	2
Number of neurons in the hidden layers	100
Activation function	ReLu
Solver for weight optimization	Adam
Regularization term	L2 penalty
Learning rate	Adaptative
Iterations	10

Table 1 MLP parameters
Source: own work [Microsoft Excel]

ISSN-On line: 2410-4191

We used this genereric MLP for PA analysis along the different amount of compression of the SI for simplicity and time reasons, probably with a more sophisticated classifier we will get higher pixel accuracies.

Experiment 2 Results

PC/TB:	PA-After PCA	PA-After TKD
8	0.64463386	0.720789813
7	0.642744424	0.718850841
6	0.646523296	0.737203847
5	0.645111526	0.72697117
4	0.642447209	0.727742513
3	0.629613904	0.720478445
2	0.604534647	0.723838032
1	0.52536055	0.687503538

Table 2 PA results along different amount of compression by PCA and TKD as a preprocessing step of semantic segmentation.
Source: own work [Python 3.7.6, Microsoft Excel]

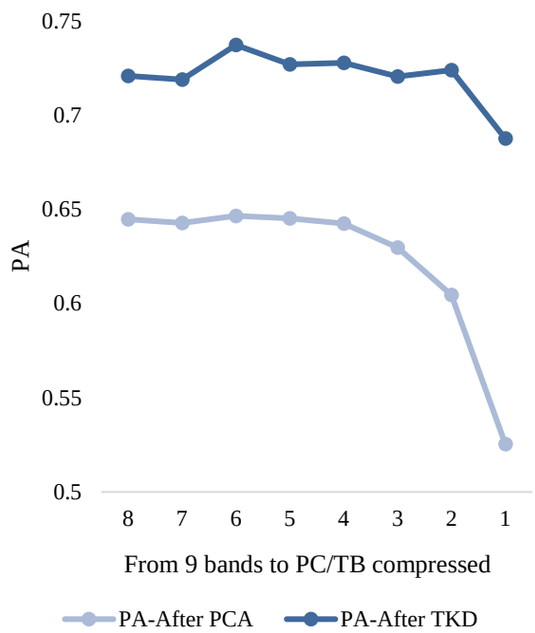

Figure 6 PA results in scatter plot along different amount of compression by PCA and TKD as a preprocessing step of semantic segmentation. A PA improve can be seen at 6 PC/TB; this increment is more notorious in TKD
Source: own work [Microsoft Excel]

Acknowledgment: to J. López for his help on the Tucker decomposition implementation and the provided dataset.

Conclusions

Generally, Tucker Decomposition can perform a better compression than Principal Component Analysis as can be seen graphically in the first experiment and numerically in the second one.

This can be seen at optimization for the Tucker Decomposition for spectral imagery compressing only on the spectral domain without matricization as in Principal Component Analysis. Thus, at the first experiment, we can see how both methods are able to reduce noise over masses of water. However, TKD preserves more information about vegetation zones. Furthermore, at the second experiment, the pixel accuracy obtained using TKD is superior than PCA in all the possible cases. For example, the PA after a TKD of six tensorial bands is higher than at seven and eighth which is related with the phenomenon seen at (López et al., 2020). Also, PCA shows this phenomenon, but with less significative results. Finally, both compression methods show poor performance with only one PC/TB respectively as expected. Therefore, future work is necessary to explain mathematically this phenomenon and its relationship with noise. This will allow to improve the classifier performance with modified state-of-the-art models for spectral image semantic segmentation with hardware accelerated implementations on TKD variants.

References

Bioucas-Dias, J. M., & Nascimento, J. M. P. (2008). Hyperspectral Subspace Identification. *IEEE TRANSACTIONS ON GEOSCIENCE AND REMOTE SENSING*, *46*(8). https://doi.org/10.1109/TGRS.2008.918089

Borengasser, M., Hungate, W., & Watkins, R. (2007). *Hyperspectral remote sensing: principles and applications*.

Jollife, I. T., & Cadima, J. (2016). Principal component analysis: A review and recent developments. In *Philosophical Transactions of the Royal Society A: Mathematical, Physical and Engineering Sciences* (Vol. 374, Issue 2065). Royal Society of London. https://doi.org/10.1098/rsta.2015.0202

Kolda, T. G., & Bader, B. W. (2009). Tensor decompositions and applications. In *SIAM Review* (Vol. 51, Issue 3, pp. 455–500). https://doi.org/10.1137/07070111X

ISSN-On line: 2410-4191

Kong, X., Zhao, Y., Xue, J., & Chan, J. C.-W. (2019). Hyperspectral Image Denoising Using Global Weighted Tensor Norm Minimum and Nonlocal Low-Rank Approximation. *Remote Sensing*, *11*(19), 2281. https://doi.org/10.3390/rs11192281

Landgrebe, D. A., & Makaret, E. (1986). Noise in Remote-Sensing Systems: The Effect on Classification Error. *IEEE Transactions on Geoscience and Remote Sensing*, *GE-24*(2), 294–300. https://doi.org/10.1109/TGRS.1986.289648

López, J., Torres, D., Santos, S., & Atzberger, C. (2020). Spectral Imagery Tensor Decomposition for Semantic Segmentation of Remote Sensing Data through Fully Convolutional Networks. *Remote Sensing*, *12*(3), 517. https://doi.org/10.3390/rs12030517

Rasti, B., Scheunders, P., Ghamisi, P., Licciardi, G., & Chanussot, J. (2018). Noise Reduction in Hyperspectral Imagery: Overview and Application. *Remote Sensing*, *10*(3), 482. https://doi.org/10.3390/rs10030482
.

ISSN-On line: 2410-4191

Article **ECORFAN Journal-Bolivia**
June 2020 Vol.7 No.12 17-22

Synthesis and incorporation of ZnO/TiO_2 in PMMA to study its thermal properties

Síntesis e incorporación de ZnO/TiO_2 en PMMA para estudio de sus propiedades térmicas

GAYTÁN-LARA, Francisco Javier†´, ZÁRRAGA–NUÑEZ Ramón´ and GALINDO-GONZÁLEZ, Rosario´´

´Universidad de Guanajuato, Division of Natural and Exact Sciences, Noria Alta S / N, Col. Noria Alta, C.P. 36050, Guanajuato, Guanajuato, Mexico.
´´CONACYT Chair Universidad de Guanajuato, Division of Natural and Exact Sciences.

ID 1st Author: *Francisco Javier, Gaytán-Lara* / **ORC ID:** 0000-0001-9007-254X, **CVU CONACYT ID:** 1006733

ID 1st Coauthor: *Ramón, Zárraga-Nuñez* / **ORC ID:** 0000-0002-7659-0743, **CVU CONACYT ID:** 38700

ID 2nd Coauthor: *Rosario, Galindo-González* / **ORC ID:** 0000-0002-3612-1555, **CVU CONACYT ID:** 223987

DOI: 10.35429/EJB.2020.12.7.17.22 Received: January 10, 2020; Accepted: June 25, 2020

Abstract

The creation of films formed by the incorporation of ZnO or TiO_2 in poly(methylmethacrylate) PMMA matrices was proposed in order to improve their properties as resistance to high temperatures. ZnO and TiO_2 nanoparticles were synthesized by the sol-gel method, which does not require the use of surfactants and is easily scalable. In the present work, zinc oxide (ZnO) or titanium oxide (TiO_2) incorporations were carried out in a polymeric matrix of Poly(methylmethacrylate) PMMA. Both oxides were characterized by Fourier transform infrared spectroscopy (FTIR), X-ray diffraction spectroscopy (XRD) and diffuse reflectance UV-Vis spectroscopy. PMMA was obtained by the suspension free radical polymerization method and PMMA composites containing ZnO or TiO_2 were obtained. Polymer characterization was performed using Fourier transform infrared spectroscopy (FTIR). The composites were analyzed by thermogravimetric analysis (TGA) and its thermal resistance was found to be the best incorporation of TiO_2 in 1%.

PMMA, Suspension Polymerization, ZnO, TiO_2

Resumen

Se propuso la creación de películas formadas por la incorporación de ZnO ó TiO_2 en matrices de PMMA con el fin de mejorar sus propiedades como resistencia a altas temperaturas. Las nanopartículas de ZnO y TiO_2 se sintetizaron por el método sol-gel, el cual no requiere el uso de tensoactivos y es fácilmente escalable. En el presente trabajo se llevaron a cabo incorporaciones de óxido de zinc (ZnO) u óxido de titanio (TiO_2) en una matriz polimérica de Polimetacrilato de metilo PMMA. Ambos óxidos fueron caracterizados por espectroscopía infrarroja por transformada de Fourier (FTIR), espectroscopía de difracción de rayos-X (DRX) y espectroscopía UV-Vis de reflectancia difusa. El PMMA se obtuvo por el método de polimerización por radicales libres en suspensión y se obtuvieron compositos de PMMA conteniendo ZnO ó TiO_2. La caracterización del polímero se realizó mediante la técnica, espectroscopía infrarroja por transformada de Fourier (FTIR). Se analizaron los compositos mediante análisis termogravimétrico (TGA) y se encontró que aumenta su resistencia térmica siendo la mejor incorporación la de TiO_2 en 1%.

PMMA, Polimerización en Suspensión, ZnO, TiO_2

Citation: GAYTÁN-LARA, Francisco Javier, ZÁRRAGA–NUÑEZ Ramón and GALINDO-GONZÁLEZ, Rosario. Synthesis and incorporation of ZnO/TiO_2 in PMMA to study its thermal properties. ECORFAN Journal-Bolivia. 2020. 7-12:17-22.

† Researcher contributing as first author.

Introduction

The polymer industry is one of the most active sectors in the world economy due to the sustained demand of its products in many technological applications.

Synthetic polymers have become an essential part of our daily lives by being part of various objects and materials with which we are in contact throughout the day. Its great variety and numerous applications, increasingly specific and of greater added value in different areas such as electronics, optics and biomedical, have made polymer science an area with a lot of research and innovation potential both academic and industrial [I].

Poly(methylmethacrylate) PMMA is a well-known amorphous polymer (mainly), it has two asymmetric side groups along the spine: methyl ($–CH_3$) and polar and larger ester ($–COOCH_3$) side groups [II].

It is an important member of the family of polyacrylic and methacrylic esters. It has several desirable properties, including exceptional optical clarity, good weather resistance, high strength and excellent dimensional stability [III].

Polymers are characterized by having two types of main transition temperatures: the crystalline melting temperature Tm (or crystalline melting point) and the glass transition temperature Tg.

The crystalline melting temperature is the melting temperature of the crystalline domains of a polymer sample. The glass transition temperature is the temperature at which the amorphous domains of a polymer assume the characteristic properties of the glassy state such as fragility, hardness and stiffness.

The values of Tg and Tm of a polymer affect its mechanical properties at any particular temperature and determine the range of temperatures at which the polymer can be used.

Some of the factors that decrease the tendency to crystallize a polymer also lead to an increase in the values of Tm (and also Tg).

The reason for this is that the degree of crystallinity developed in a polymer is controlled both kinetically and thermodynamically, while the melting temperature is controlled only thermodynamically. Polymers with rigid chains are difficult or slow to crystallize, but the portion that crystallizes will have a high melting temperature.

Ceramic materials are usually designed for use at high temperatures, their resistance to thermal creep is a very important property. Thus, the crystalline ceramics have a resistance to thermal creep due to their high melting points.

ZnO is a ceramic photoactive material that at its nanometric scale sees its properties enhanced. TiO_2 is an inorganic ceramic material widely used in the industry due to its optical, mechanical and chemical properties, as well as its relative accessibility.

Sol-Gel Method

The sol-gel method involves a colloidal suspension of particles where the precursor can be an alkoxide metal such as an aluminate, titanate, borate, silicate, thiosulfate, among the most commonly used. The sol-gel method is a technique that leads to the formation of oxides by polymeric inorganic reactions. It has 4 characteristic stages: hydrolysis, polycondensation, drying and thermal decomposition [IV]. Therefore, its advantages of the Sol-Gel method are the ease and the low temperature of synthesis [V].

Suspension Polymerization

In suspension polymerization the initiator is soluble in the monomer (dispersed phase) which in turn is immiscible in water (continuous phase), which contains the stabilizing agent and which is soluble in it. It is important to mention that it is important to maintain a stir in the system; likewise, the stabilizer hinders the coalescence of monomer droplets and polymer particles, whose tendency to agglomerate can cause problems [VI]. A reverse suspension polymerization involves an organic solvent as a continuous phase, with dispersed drops of a water soluble monomer (acrylamide, acrylic acid and soluble acrylates), which may be pure or dissolved in water, and the initiator.

ISSN-On line: 2410-4191

Commonly used items made of polymers undergo modifications are favored by the isolated or combined action of certain environmental conditions, for example wear (yellowing) due to UV radiation as well as deformation due to heat.

This significantly decreases its useful life, therefore, it is important to implement a technological route to prolong the useful life of polymers, mainly diminished by their interaction with ultraviolet radiation and high temperatures.

It is reported that zinc oxide and titanium dioxide have an excellent absorption of UV radiation, with application in different industries, their incorporation in polymeric matrices to manufacture composites can achieve that their properties (thermal resistance, resistance to photodegradation), Be remarkably improved.

Therefore, this work was aimed at finding a composite that gives better thermal resistance to PMMA by making 2 different types, one incorporating ZnO and the other with TiO_2.

At the same time looking for what proportion gives better results between the options 1% and 0.3%.

Thus, the hypothesis was that the incorporation of the metal oxides ZnO or TiO_2 in the polymeric matrices of PMMA will make a synergy relationship improving the properties of the polymer films. In particular, a higher thermal resistance is expected.

Methodology

For ZnO synthesis a 0.06 M solution of zinc acetate Zn $(CH_3COO)\ 2 \cdot (H_2O)_2$ in 400 mL of methanol (CH_3CH_2OH) and a 0.5 M solution of sodium hydroxide (NaOH) in 250 mL of methanol were prepared. The zinc acetate solution was placed in an Erlenmeyer flask under constant magnetic stirring at 800 rpm and the NaOH solution was added dropwise to adjust to a pH = 11. The flask was then placed in an oil bath at a temperature of 60 °C maintaining magnetic stirring at 800 rpm for 1h. After the time elapsed, the reaction flask was immediately subjected to an ice bath for 20 minutes to stop the growth [VII].

The nanoparticles were recovered in 50 mL Falcon tubes subjected to centrifugation at 6000 rpm for 20 min. At the end of the centrifugation, methanol was discarded and the recovered nanoparticles were placed in a crucible which was left for 12 hours at 60 ℃ in a convection oven. Finally, the crucible was placed in a flask at 100 °C for 1 hour.

TiO_2 nanoparticles were obtained through the aging process accompanied by hydrolysis/polycondensation.

Titanium tetraisopropoxide (TTIP) was used as the starting material. 5 mL of TTIP and H_2O in a molar ratio of 100 H_2O/Ti were placed in a flask, the reaction flask was subjected to constant magnetic stirring at 1000 rpm and temperature of 90 °C (using a cooling system to prevent evaporation of H_2O). The reaction was allowed to be carried out for 72 hours, taking care to keep the temperature constant after the first 30 minutes, which were critical to stabilize the reaction and thus optimize aging. The TiO_2 solution will be transformed into a one-phase paste solution, and a peptizing agent was added, in this case HNO_3 at a molar ratio of 0.25 HNO_3/Ti. For the preparation of the TiO_2 powder, the solution was dried at 100 ° C for 24 h in a convection oven and finally calcined at 500 °C for 2h in a flask. Finally the powder was ground in agate mortar [VIII].

To perform the synthesis of PMMA by the free radical polymerization method in suspension, glycerol was used as a continuous medium and as a microcrystalline cellulose dispersing medium (DS-0 cellulose powder), placed in a beaker at 75 °C and magnetic stirring constant at 380 rpm, adding as initiator benzoyl peroxide (BPO) dissolved in the monomer (methyl methacrylate) [IX].

NOTE: For the incorporations, the ZnO or TiO_2 nanoparticles (which were previously sonicated for 30 min in a glass with 3 mL of methanol) were added at the beginning of the polymerization.

Sample	Matrix	% ZnO	% TiO_2
1	PMMA	0	0
2	PMMA	0.3	0
3	PMMA	1	0
4	PMMA	0	0.3
5	PMMA	0	1

Table 1 Synthesized samples

ISSN-On line: 2410-4191

Results

FTIR

The spectrum of the PMMA sample shows that the bands at 2997, 2951 and 2845 cm^{-1} are due to CH type elongation vibrations of methyl and methylene, the band at 1732 cm^{-1} is due to a stretch C = Or of the ester group present in the PMMA, the bands in 1483,1450,1437 and 1387 cm^{-1} are due to deformation vibrations of CH bonds typical of PMMA methyl and methylene, the bands in 1271 and 1242 cm^{-1} are due At the C–O elongation of the ether group, the 1194 and 1150 cm^{-1} bands are due to vibrations of the CH flap and torsion link out of plane respectively, the 1061 cm^{-1} band is due to a C-OH bond due to to possible presence of glycerol). The 989 cm^{-1} band is due to the elongation of the DC link, the 841 cm^{-1} band is due to the rolling methylene vibration in the plane and the 750 cm^{-1} band is due to the C=O vibration link torsion out of plane [X].

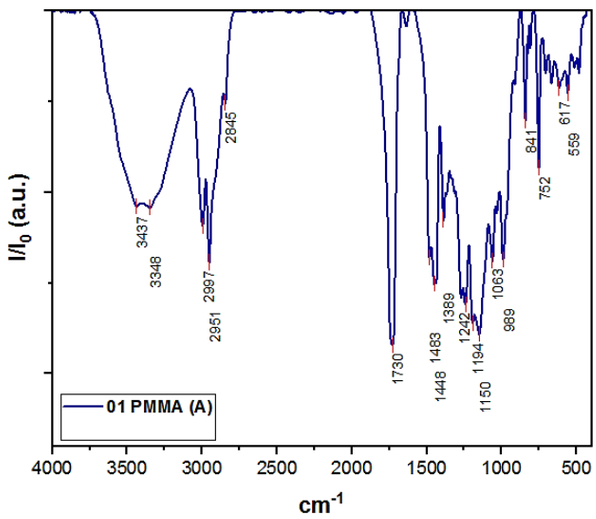

Graphic 1 Infrared spectrum in KBr plates for the sample 1 PMMA in chloroform

The spectrum of the ZnO sample shows a peak is observed in 482 cm^{-1} belonging to the stretch band of the Zn-O bond, the peak of 841 cm^{-1} belongs to the Zn-Zn bond and corresponds to the tetrahedral coordination of Zn, the peak in 1086 cm^{-1} it is due to the elongation band of the zinc acetate precursor. The peaks in 1439 cm^{-1}, 1512 cm^{-1} and 1560 cm^{-1} are due to symmetric and asymmetric stretching vibrations C=O probably of zinc acetate precursor, finally the weak wide peak in 3339 cm^{-1} is due to OH stretch vibration [XI].

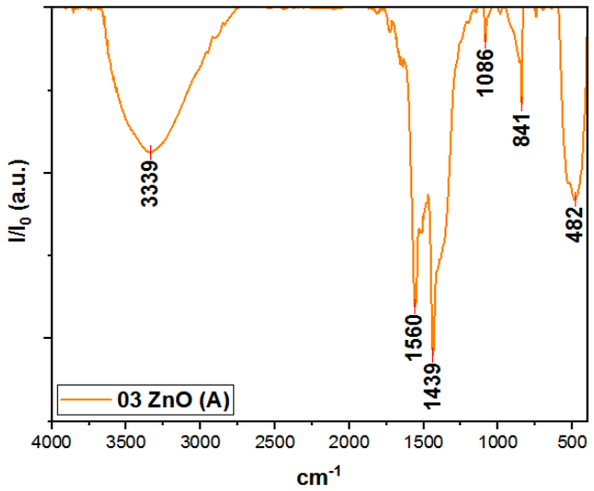

Graphic 2 Infrared spectrum in KBr plates for sample ZnO in MeOH

The spectrum of the TiO_2 sample shows a peak in 669 cm^{-1} of the Ti-O-O bond which confirms the presence of titanium dioxide. In addition, the signals in 3381cm^{-1} and 1620 cm^{-1} belonging to the O-H and N = O bonds of the nitric acid used in the synthesis of TiO_2 can be observed.

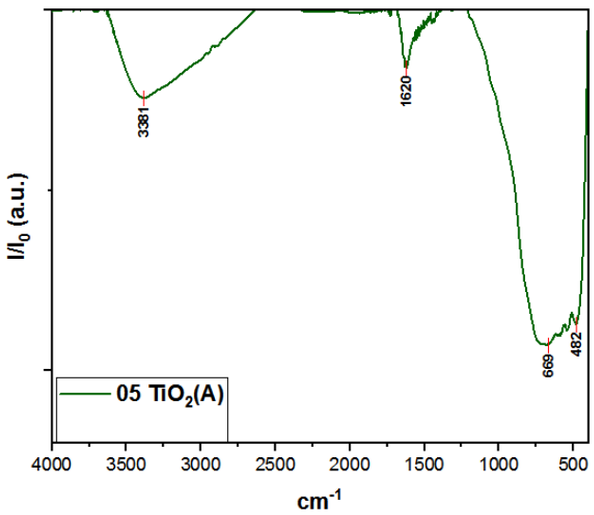

Graphic 3 Spectrum in KBr plates for sample TiO_2 in MeOH

DRX

From the X-ray diffraction it is possible to determine the crystallite size. Scherrer's formula was used to calculate crystallite size using the equation:

$$B = \frac{K\lambda}{L\cos\theta} \quad (1)$$

ISSN-On line: 2410-4191

Sample	Position 2θ (°)	B (FWHM)	Crystal size L (nm)
ZnO	36.29	0.29	37.35
TiO_2	25.25	0.88	10.37

Table 2 Crystal size calculations using the Scherrer equation with values of XRD.

Diffuse reflectance UV-Vis

For TiO_2 sample it is reported that the experimental values obtained from Band gap (Egap) are due to the high synthesis temperature (90 ° C) since lowering the temperature results in higher values of Egap [XII].

Sample	Theoretical Egap (eV)	Experimental Egap (eV)
ZnO	3.37	3.09
TiO_2	2.8 – 3.3	3.15

Table 2 Comparison between the theoretical and experimental band gap calculated

TGA.

The TGA shows that the thermal resistance of PMMA-ZnO (for 0.3% and 1%) increases, at 308 °C the loss of mass was reduced 11%, the decomposition of most mass goes from 448 °C to 462 °C, while for PMMA-TiO_2 the thermal resistance increases, going from breaking down the PMMA from 448 °C to 455 for 0.3% or up to 460 °C for 1%.

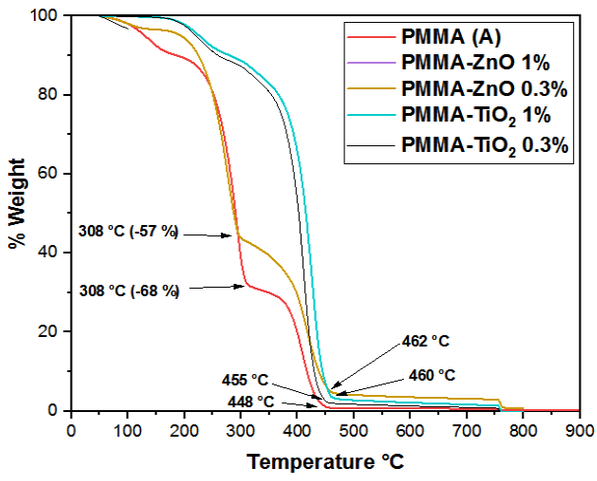

Graphic 4 TGA studies for samples PMMA, PMMA-ZnO and PMMA-TiO_2

Conclusions

The sol gel method is a good method for synthesis of nanoparticles of metal oxides (ZnO and TiO_2) since it is simple, with a high level of conversion and cheap, making it a scalable process. The polymer with the highest thermal resistance was with 1% TiO_2 which showed a difference greater than 100 °C to begin most thermal decomposition.

Acknowledgments

This project was conducted under the results from project IJ – 236 -2019.

IPICYT for conducting TGA studies.

National laboratory for the characterization of physicochemical properties and molecular structure, University of Guanajuato.

References

I. Contreras L., D.; Saldívar-G., E. & Luna-B., G. 2013. “Copolymerization of isoprene with polar vinyl monomers: Reactivity ratios, characterization and thermal properties.” European Polymer Journal 49, 2013, 1760–1772.

II. Behbahani, A.F.; Vaez-Allaei, S.M.; Motlagh, G.; Eslami, H. & Harmandaris, V. 2018. "Structure and dynamics of stereo-regular poly(methyl-methacrylate) melts through atomistic molecular dynamics simulations." Soft Matter, 2018, 14, 1449.

III. Huang, X. & Brittain, W. 2001. "Synthesis and Characterization of PMMA Nanocomposites by Suspension and Emulsion Polymerization" Macromolecules 2001, 34, 3255-3260.

IV. Shipra-Mital, Gupta, Manoj, Tripathi. 2011 "A review on the synthesis of TiO_2 nanoparticles by solution route." Central European Journal of Chemistry · August 2011.

ISSN-On line: 2410-4191

V. Shaban, M.; Abdallah, S. & Abdel-K. A. 2016. "Characterization and photocatalytic properties of cotton fibers modified with ZnO nanoparticles using sol–gel spin coating technique" Beni-suef university journal of basic and applied sciences 5, 2016 277–283.

VI. Kalfas, G. y Ray, W. H. 1993. "Modeling and experimental studies of aqueous suspension polymerization processes." Industrial and Engineering Chemistry Research, 32(9):1822-1830.

VII. López V. A. 2015. "Crecimiento de nanoalambres de óxido de zinc verticalmente alineados usando el método sol-gel hidrotermal." BUAP.

VIII. Kyung-Jun, Hwang; Jae-Wook, Lee; Wang-Geun, Shim; Hee, Dong, Se-Il, Lee & Seung-Joon, Yoo. 2012. "Adsorption and photocatalysis of nanocrystalline TiO_2 particles prepared by sol–gel method for methylene blue degradation" Advanced Powder Technology 23 (2012) 414–418.

IX. Santa María, L.C.; Aguiar, M.R.M.P.; D'Elia, P.; Ferreira, L.O. & Wang, S.H. 2006. "The incorporation of polar monomers in copolymers based on styrene and divinylbenzene obtained from glycerol suspension polymerization." Materials Letters 61, 160–164.

X. Abdelghany, A.M.; Abdelrazek, M.; ElShahawy A. & Al-Muntaser, A.A. 2015. "FTIR and UV/Vis. Spectroscopy: A Key for Miscibility Investigation of PVC/PMMA Polymer Blend." Middle East J. Appl. Sci., 5(4): 36-44, 2015.

XI. Rodriguez M., C.; Joshi, P.; Vera, J.L.; Ramirez-Vick, J.E.; Perales, O. & Singh, S.P. 2011. "Cytotoxic studies of PEG functionalized ZnO nanoparticles on MCF-7 cancer Cells." Research Gate, January 2011.

XII. Selman, A.M. & Hassan, Z. 2013. "Influence of deposition temperature on the growth of rutile TiO_2 nanostructures by CBD method on seed layer prepared by RF magnetron sputtering." Superlattices and Microstructures 64 (2013) 27–36.

ISSN-On line: 2410-4191

Article **ECORFAN Journal-Bolivia**
June 2020 Vol.7 No.12 23-27

Magnetite coupling in a PS/PMMA block copolymer using suspension polymerization

Acoplamiento de magnetita en un copolímero PS/PMMA usando polimerización por suspensión

CARMONA-TORRES Marco†´, FUENTES-RAMÍREZ, Rosalba´, CONTRERAS-LOPEZ, David´ and GALINDO-GONZÁLEZ, Rosario´´*

´Dept. of Chemical Engineering, Division of Natural and Exact Sciences, Universidad de Guanajuato, Noria Alta S/N, Guanajuato, Gto. México 36050
´´ CONACYT Chair Universidad de Guanajuato, Division of Natural and Exact Sciences.

ID 1st Author: *Marco, Carmona-Torres*

ID 1st Coauthor: *Rosalba, Fuentes-Ramírez* / **ORC ID:** 0000-0003-0520-3387, **CVU CONACYT ID:** 202669

ID 2nd Coauthor: *David, Contreras-Lopez* / **ORC ID:** 0000-0003-1384-4766, **CVU CONACYT ID:** 38297

ID 3rd Coauthor: *Rosario, Galindo-González* / **ORC ID:** 0000-0002-3612-1555, **CVU CONACYT ID:** 223987

DOI: 10.35429/EJB.2020.12.7.23.27 Received: January 10, 2020; Accepted: June 30, 2020

Abstract

The objective of the present article is to introduce nanoparticles of a ferromagnetic material (magnetite) to the polymer matrix. We will make some study to verify that the coupling of the nanoparticles in the material was carried out. The present work describes the self-assembly of nanocomposite in suspensión polymerization of PS/PMMA block copolymer, containing magnetite (Fe_3O_4) which is sonicated with the monomer mixture, with percentages of 0.25% and 0.5% in proportion of the weight of mixture. Photographs were taken with the microscope to verify the coupling of the ferromagnetic material to the polymer matrix, and to verify that couplig, we made characterization by infrared spectroscopy. Also describes the process of nanocomposite synthesis using co-precipitation method, in which ferric chloride and ferrous chloride are combined in an excess basic medium, to subsequently induce the precipitation of the material with a magnet.

Magnetite, Copolymer, Nanocomposite

Resumen

El objetivo del presente artículo es introducir nanoparticulas de un material ferromagnético (magnetita) a la matriz polimérica. Se efectuaron pruebas para comprobar que se llevó a cabo el acoplamiento de dichas nanopartículas en el material. En este trabajo se describe el auto ensamblaje de un nanocomposito, utilizando el método de polimerización por suspensión de una mezcla de polímeros (PS/PMMA) en combinación con magnetita (Fe_3O_4), la cual fue sonicada con la mezcla de monómeros, conteniendo porcentajes de 0.25% y 0.5% en proporción del peso de la mezcla de monómeros. Se tomaron fotografías con el microscopio para comprobar el acoplamiento del material ferromagnético a la matriz polimérica, y se llevó a cabo la caracterización mediante espectrometría infrarroja para corroborar dicho acoplamiento. También se describe el proceso de síntesis del nanocomposito utilizando el método de co-precipitación, en el cual se combinan cloruro férrico y cloruro ferroso en un medio básico en exceso, para posteriormente inducir la precipitación del material con un imán.

Magnetita, Copolímero, Nanocomposito

Citation: CARMONA-TORRES Marco, FUENTES-RAMÍREZ, Rosalba, CONTRERAS-LOPEZ, David and GALINDO-GONZÁLEZ, Rosario. Magnetite coupling in a PS/PMMA block copolymer using suspension polymerization. ECORFAN-Bolivia Journal. 2020. 7-12:23-27.

* Correspondence to Author (Email: mr.galindo@ugto.mx)
† Researcher contributing as first author.

Introduction

The objective of the present article is to introduce nanoparticles of a ferromagnetic material (magnetite) to the polymer matrix. We will make some study to verify that the coupling of the nanoparticles in the material was carried out.

Suspension polymerization is a process in which the polymerization of relatively water-insoluble monomer droplets formed by vigorous stirring in the presence of a steric stabilizer leads to an aqueous dispersion of polymer particles [1]. The interfacial tension, the degree of agitation, and the design of the stirrer/reactor system govern the dispersion of monomer droplets. The presence of suspending agents (e.g., stabilizers) hinder the coalescence of monomer droplets and the adhesion of partially polymerized particles during the course of polymerization, so that the solid beads may be produced in the same spherical form in which the monomer was dispersed in the aqueous phase [2]. Under proper experimental conditions, block copolymers, which are composed of chemically different blocks, can self- assemble at the nanometer scale, into various well-defined morphologies corresponding to the molecular dimensions of each block. Recent studies have found that incorporation of nanoparticles (NPs) into self-assembled block copolymers can greatly improve the mechanical strength, electrical conductivity, and optical properties of this composite [3], and the magnetic properties will provide future opportunities in technologies such as solar cells, photonic bandgap materials, and high-density magnetic storage devices [4].

The present work describes the self-assembly of nanocomposite in suspension polymerization of PS/PMMA block copolymer (see Figure 1), containing magnetite (Fe_3O_4) which is sonicated with the monomer mixture, with percentages of 0.25% and 0.5% in proportion of the weight of mixture. Photographs were taken with the microscope to verify the coupling of the ferromagnetic material to the polymer matrix, and to verify that coupling, we made characterization by infrared spectroscopy. Also describes the process of nanocomposite synthesis using co-precipitation method, in which ferric chloride and ferrous chloride are combined in an excess basic medium, to subsequently induce the precipitation of the material with a magnet.

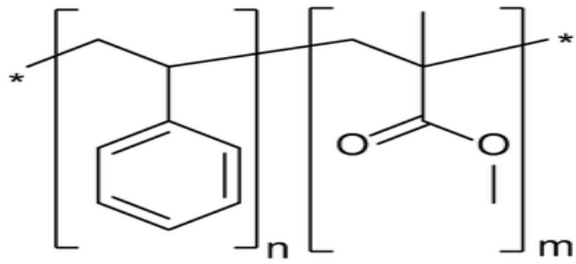

Figure 1 Structure of PS/PMMA block copolymer
Source: (Bennett et al., 2014)

Methodology

Reagents

Monomer: Styrene and methyl methacrylate with a purity percentage > 99% sigma Aldrich. We have to eliminate the inhibitors washing the monomer with sodium hydroxide 0.1 M solution.

Dispersing agent: polyvinyl alcohol (PVA).

Initiator: Benzoyl peroxide (BPO) purity percentage 97%

Polymerization of block copolymer:

We use the suspension polymerization method. The reactions were carried out in a 500 mL batch reactor, using as continuous phase 45 mL of PVA with a concentration of 5 g/L. We combined 10 mL of the monomer mixture (styrene 90%/ Methyl methacrylate 10%) with 025% and 0.5% of magnetite according with the weight of the mixture (approximately 9.09 g). After that, we sonicate the mixture with the magnetite for 10 min to disperse the particles into monomers. We added the initiator after sonicating and proceed to added it to the reactor when the PVA reach the temperature of the reaction (75 °C), with constant agitation of 130 rpm with mechanical agitation.

Time of reaction: 3 ½ hours.

Synthesis of magnetite:

For the magnetite synthesis we aggregate 100 mL of potassium hydroxide (KOH) 2M to a beaker and heat to 60 °C.

ISSN-On line: 2410-4191

For the chlorides, we prepare 10 mL of ferrous chloride ($FeCl_2$) 0.1 M and 10 mL of ferric chloride ($FeCl_3$) 0.05 M and were added drop by drop with constant agitation.

After 30 minutes, we turn off the heating and precipitate the magnetite with a magnet, adding ethanol to wash the remanent water. After that, we put the magnetite on a stove to dry it.

Results

A TEM microscopy obtained at a resolution of 50 nm is shown in Figure 2, a magnetite with an average size of 30 nm being observed, spherical and denoting that the particles are structurally homogeneous.

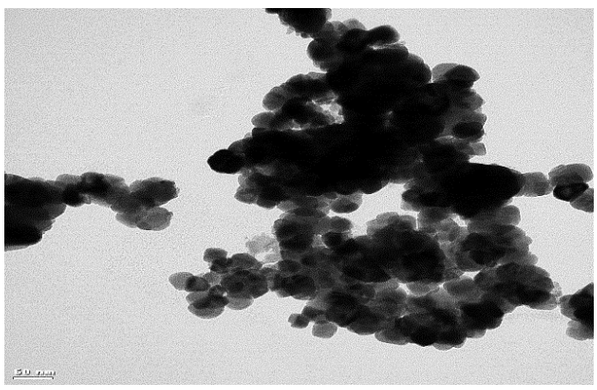

Figure 2 TEM Microscopy of magnetite

As can be seen in Graphic 1, a comparison made with the theoretical structure of magnetite (blue dots) and the experimentally elaborated (red curve), showing that the peaks coincide in 99%, being at the peak that is a value of 2Θ of 36 where Fe is found.

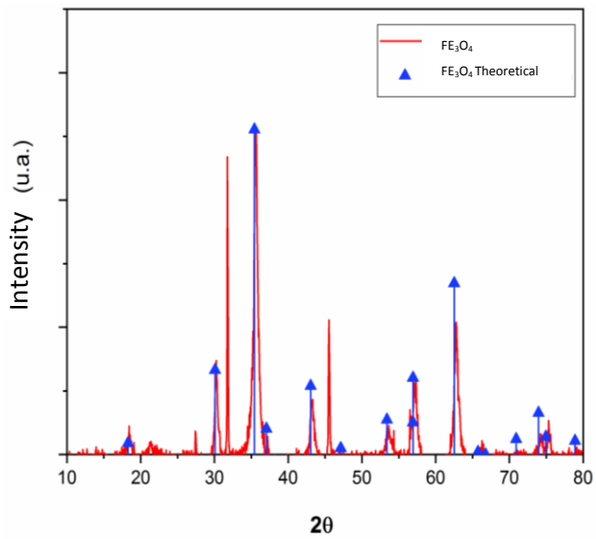

Graphic 1 X-ray diffractogram comparing Theoretical vs Experimental magnetite

The FT-IR spectra that verify the presence of Fe_3O_4 are observed in Graphic 2. It was carried out on KBr plates since they allow to visualize the part of the spectrum that goes from 4000 to 400 cm^{-1} and ZnO has between 650- 720 cm-1 its characteristic peak of the Fe-O bond using MeOH to disperse them.

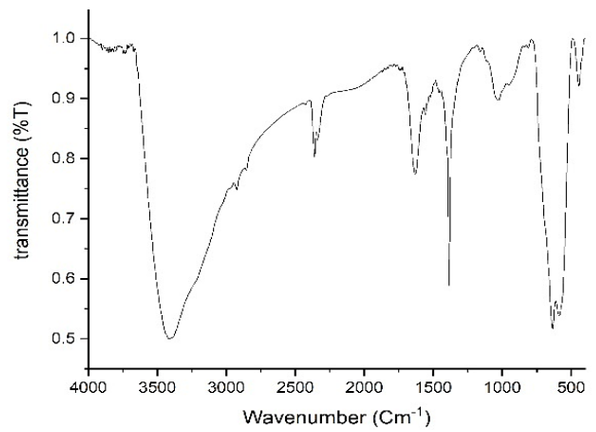

Graphic 2 Magnetite IR spectrum

Graphic 3 shows the infrared spectrum of copolymer polystyrene/methyl methacrylate. In this case, band of an aromatic monosubstituted is in region to 1940-1745 cm^{-1}, bands of stretching C-H bonds between 3080-3090 cm^{-1}, bands of stretching CH_2 bonds between 2920-2850 cm^{-1} and band between 750 to 690 cm^{-1} corresponds to the mono-substitution of the ring. Perhaps, 1600 cm^{-1} correspond the bond C=C and between 1490-1450 cm^{-1} the bond C-C. The bands of the C-H bonds between 3000 to 2870 cm^{-1} band, at 1730 cm^{-1} due to the presence of carbonyl groups C=O and between 1060-1120 cm^{-1} the C-O link.

ISSN-On line: 2410-4191

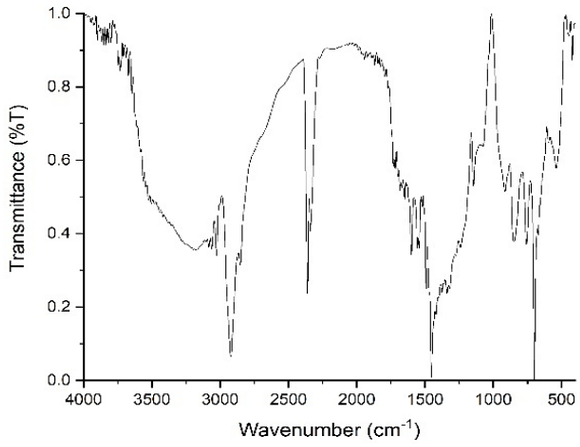

Graphic 3 PS/PMMA block coplymer IR spectrum

As can be seen in Graphics 4 and 5, the band in 2900 cm^{-1} shows a polymer peak where in the different percentages of magnetite. The higher percentage decreases and moves to 2800 cm^{-1}, the other peak that decreases is between 1800-1600 cm^{-1} where the two peaks in the percentages 0.5 and 0.25 while in the 700 cm^{-1} where the magnetite is found. It is observed that the peak is growing as it decreases in the percentage amount of magnetite these, it should be that the incorporations causes the methacrylate molecules to tense due to this it can be said that the magnetic particles are within the polymeric matrices.

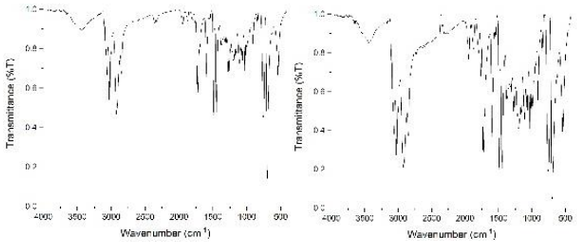

Graphic 4 PS/PMMA block copolymer coupling with magnetite 0.5% IR spectrum A) without sonication and B) sonicated

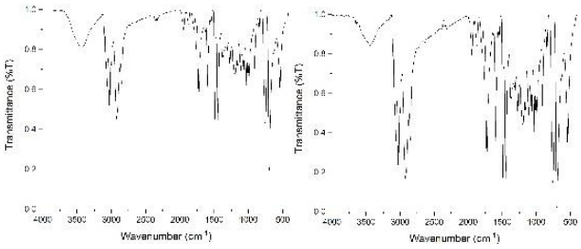

Graphic 5 PS/PMMA block copolymer coupling with magnetite 0.25% IR spectrum A) without sonication and B) sonicated

Likewise, the effect of the dispersion process via physical mixing by sonication and the *in-situ* process during the polymerization process can be seen in both graphics.

Conclusions

By means of the ultrasonic bath it is possible to obtain magnetic polymeric nanocomposites, with good stability for their applications. The stability and dispersion of polymeric nanocomposites depends on the molecular weight and viscosity of the polymer. At low viscosities, the nanoparticles disperse easily but are less stable than at high viscosities although dispersion requires more time.

The IR spectrum show us the incorporation of the ferromagnetic material with the block copolymer. The presence of the pick on the 700 cm^{-1} region it´s characteristic of the magnetite, which is present in the Graphics 3, 4 and 5.

In the Graphics 4B and 5B we can prove than the process of sonication helps us increasing the coupling of the magnetite with the polymeric matrix, decreasing the percentage of transmittance in comparison of the Graphics 4A and 5A.

Acknowledgement

We are grateful to project 144 of the CIIC-UGTO-2020 call (Obtaining polymeric nanocomposites via heterophasic polymerization processes for the development of surface protection).

References

[1] H. Gonçalves, O., M. Asua, J., Henrique Hermes de Araújo, P., & A. F. Machado, R. (2008). Synthesis of PS/PMMA Core−Shell Structured Particles by Seeded Suspension Polymerization. *Macromolecules*, *41*(19), 6960–6964. https://doi.org/10.1021/ma800693m

[2] Vivaldo-lima, E., Wood, P. E., Hamielec, A. E., Penlidis, A., & Equation, P. B. (1997). *An Updated Review on Suspension Polymerization*. *5885*(905), 939–965. https://doi.org/10.1021/ie960361g

ISSN-On line: 2410-4191

[3] Yang, P., Wang, S., Teng, X., Wei, W., Dravid, V. P., & Huang, L. (2012). Effect of magnetic nanoparticles on the morphology of polystyrene- b-poly(methyl methacrylate) diblock copolymer thin film. *Journal of Physical Chemistry C*, *116*(43), 23036–23040. https://doi.org/10.1021/jp305827x

[4] Xu, C., Ohno, K., Ladmiral, V., Milkie, D. E., Kikkawa, J. M., & Composto, R. J. (2009). Simultaneous block copolymer and magnetic nanoparticle assembly in nanocomposite films. *Macromolecules*, *42*(4), 1219–1228. https://doi.org/10.1021/ma8022266

ISSN-On line: 2410-4191

[Title in Times New Roman and Bold No. 14 in English and Spanish]

Surname (IN UPPERCASE), Name 1st Author†*, Surname (IN UPPERCASE), Name 1st Coauthor, Surname (IN UPPERCASE), Name 2nd Coauthor and Surname (IN UPPERCASE), Name 3rd Coauthor

Institutional Affiliation of Author including Dependency (No.10 Times New Roman and Italic)

International Identification of Science - Technology and Innovation

ID 1st Author: (ORC ID - Researcher ID Thomson, arXiv Author ID - PubMed Author ID - Open ID) and CVU 1st author: (Scholar-PNPC or SNI-CONACYT) (No.10 Times New Roman)

ID 1st Coauthor: (ORC ID - Researcher ID Thomson, arXiv Author ID - PubMed Author ID - Open ID) and CVU 1st coauthor: (Scholar or SNI) (No.10 Times New Roman)

ID 2nd Coauthor: (ORC ID - Researcher ID Thomson, arXiv Author ID - PubMed Author ID - Open ID) and CVU 2nd coauthor: (Scholar or SNI) (No.10 Times New Roman)

ID 3rd Coauthor: (ORC ID - Researcher ID Thomson, arXiv Author ID - PubMed Author ID - Open ID) and CVU 3rd coauthor: (Scholar or SNI) (No.10 Times New Roman)

(Report Submission Date: Month, Day, and Year); Accepted (Insert date of Acceptance: Use Only ECORFAN)

Abstract (In English, 150-200 words)

Objectives
Methodology
Contribution

Keywords (In English)

Indicate 3 keywords in Times New Roman and Bold No. 10

Abstract (In Spanish, 150-200 words)

Objectives
Methodology
Contribution

Keywords (In Spanish)

Indicate 3 keywords in Times New Roman and Bold No. 10

Citation: Surname (IN UPPERCASE), Name 1st Author, Surname (IN UPPERCASE), Name 1st Coauthor, Surname (IN UPPERCASE), Name 2nd Coauthor and Surname (IN UPPERCASE), Name 3rd Coauthor. Paper Title. ECORFAN Journal-Bolivia. Year 1-1: 1-11 [Times New Roman No.10]

* Correspondence to Author (example@example.org)
† Researcher contributing as first author.

Introduction

Text in Times New Roman No.12, single space.

General explanation of the subject and explain why it is important.

What is your added value with respect to other techniques?

Clearly focus each of its features

Clearly explain the problem to be solved and the central hypothesis.

Explanation of sections Article.

Development of headings and subheadings of the article with subsequent numbers

[Title No.12 in Times New Roman, single spaced and bold]

Products in development No.12 Times New Roman, single spaced.

Including graphs, figures and tables-Editable

In the article content any graphic, table and figure should be editable formats that can change size, type and number of letter, for the purposes of edition, these must be high quality, not pixelated and should be noticeable even reducing image scale.

[Indicating the title at the bottom with No.10 and Times New Roman Bold]

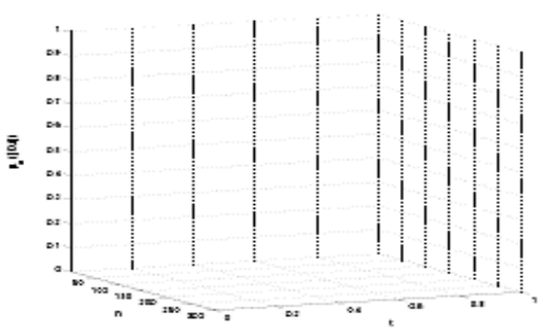

Graphic 1 Title and *Source (in italics)*

Should not be images-everything must be editable.

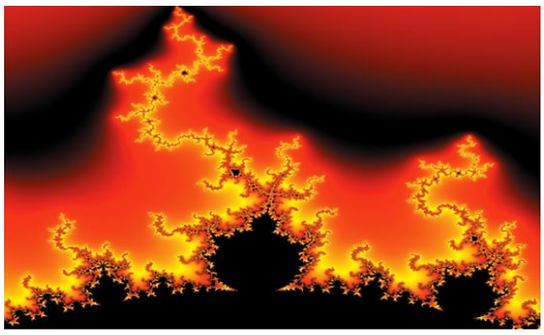

Figure 1 Title and *Source (in italics)*

Should not be images-everything must be editable.

Table 1 Title and *Source (in italics)*

Should not be images-everything must be editable.

Each article shall present separately in **3 folders**: a) Figures, b) Charts and c) Tables in .JPG format, indicating the number and sequential Bold Title.

For the use of equations, noted as follows:

$$Y_{ij} = \alpha + \sum_{h=1}^{r} \beta_h X_{hij} + u_j + e_{ij} \quad (1)$$

Must be editable and number aligned on the right side.

Methodology

Develop give the meaning of the variables in linear writing and important is the comparison of the used criteria.

Results

The results shall be by section of the article.

Annexes

Tables and adequate sources

Thanks

Indicate if they were financed by any institution, University or company.

Conclusions

Explain clearly the results and possibilities of improvement.

ISSN 2410-4191

References

Use APA system. Should not be numbered, nor with bullets, however if necessary numbering will be because reference or mention is made somewhere in the Article.

Use Roman Alphabet, all references you have used must be in the Roman Alphabet, even if you have quoted an Article, book in any of the official languages of the United Nations (English, French, German, Chinese, Russian, Portuguese, Italian, Spanish, Arabic), you must write the reference in Roman script and not in any of the official languages.

Technical Specifications

Each article must submit your dates into a Word document (.docx):

Journal Name
Article title
Abstract
Keywords
Article sections, for example:

1. Introduction
2. Description of the method
3. Analysis from the regression demand curve
4. Results
5. Thanks
6. Conclusions
7. References

Author Name (s)
Email Correspondence to Author
References

Intellectual Property Requirements for editing:

-Authentic Signature in Color of Originality Format Author and Coauthors

-Authentic Signature in Color of the Acceptance Format of Author and Coauthors

ISSN 2410-4191

Reservation to Editorial Policy

ECORFAN-Journal Bolivia reserves the right to make editorial changes required to adapt the Articles to the Editorial Policy of the Journal. Once the Article is accepted in its final version, the Journal will send the author the proofs for review. ECORFAN® will only accept the correction of errata and errors or omissions arising from the editing process of the Journal, reserving in full the copyrights and content dissemination. No deletions, substitutions or additions that alter the formation of the Article will be accepted.

Code of Ethics - Good Practices and Declaration of Solution to Editorial Conflicts

Declaration of Originality and unpublished character of the Article, of Authors, on the obtaining of data and interpretation of results, Acknowledgments, Conflict of interests, Assignment of rights and Distribution.

The ECORFAN-Mexico, S.C Management claims to Authors of Articles that its content must be original, unpublished and of Scientific, Technological and Innovation content to be submitted for evaluation.

The Authors signing the Article must be the same that have contributed to its conception, realization and development, as well as obtaining the data, interpreting the results, drafting and reviewing it. The Corresponding Author of the proposed Article will request the form that follows.

Article title:

– The sending of an Article to ECORFAN -Journal Bolivia emanates the commitment of the author not to submit it simultaneously to the consideration of other series publications for it must complement the Format of Originality for its Article, unless it is rejected by the Arbitration Committee, it may be withdrawn.

– None of the data presented in this article has been plagiarized or invented. The original data are clearly distinguished from those already published. And it is known of the test in PLAGSCAN if a level of plagiarism is detected Positive will not proceed to arbitrate.

– References are cited on which the information contained in the Article is based, as well as theories and data from other previously published Articles.

– The authors sign the Format of Authorization for their Article to be disseminated by means that ECORFAN-Mexico, S.C. In its Holding Bolivia considers pertinent for disclosure and diffusion of its Article its Rights of Work.

– Consent has been obtained from those who have contributed unpublished data obtained through verbal or written communication, and such communication and Authorship are adequately identified.

– The Author and Co-Authors who sign this work have participated in its planning, design and execution, as well as in the interpretation of the results. They also critically reviewed the paper, approved its final version and agreed with its publication.

– No signature responsible for the work has been omitted and the criteria of Scientific Authorization are satisfied.

– The results of this Article have been interpreted objectively. Any results contrary to the point of view of those who sign are exposed and discussed in the Article.

Copyright and Access

The publication of this Article supposes the transfer of the copyright to ECORFAN-Mexico, SC in its Holding Bolivia for its ECORFAN-Journal Bolivia, which reserves the right to distribute on the Web the published version of the Article and the making available of the Article in This format supposes for its Authors the fulfilment of what is established in the Law of Science and Technology of the United Mexican States, regarding the obligation to allow access to the results of Scientific Research.

Article Title:

Name and Surnames of the Contact Author and the Coauthors	Signature
1.	
2.	
3.	
4.	

Principles of Ethics and Declaration of Solution to Editorial Conflicts

Editor Responsibilities

The Publisher undertakes to guarantee the confidentiality of the evaluation process, it may not disclose to the Arbitrators the identity of the Authors, nor may it reveal the identity of the Arbitrators at any time.

The Editor assumes the responsibility to properly inform the Author of the stage of the editorial process in which the text is sent, as well as the resolutions of Double-Blind Review.

The Editor should evaluate manuscripts and their intellectual content without distinction of race, gender, sexual orientation, religious beliefs, ethnicity, nationality, or the political philosophy of the Authors.

The Editor and his editing team of ECORFAN® Holdings will not disclose any information about Articles submitted to anyone other than the corresponding Author.

The Editor should make fair and impartial decisions and ensure a fair Double-Blind Review.

Responsibilities of the Editorial Board

The description of the peer review processes is made known by the Editorial Board in order that the Authors know what the evaluation criteria are and will always be willing to justify any controversy in the evaluation process. In case of Plagiarism Detection to the Article the Committee notifies the Authors for Violation to the Right of Scientific, Technological and Innovation Authorization.

Responsibilities of the Arbitration Committee

The Arbitrators undertake to notify about any unethical conduct by the Authors and to indicate all the information that may be reason to reject the publication of the Articles. In addition, they must undertake to keep confidential information related to the Articles they evaluate.

Any manuscript received for your arbitration must be treated as confidential, should not be displayed or discussed with other experts, except with the permission of the Editor.

The Arbitrators must be conducted objectively, any personal criticism of the Author is inappropriate.

The Arbitrators must express their points of view with clarity and with valid arguments that contribute to the Scientific, Technological and Innovation of the Author.

The Arbitrators should not evaluate manuscripts in which they have conflicts of interest and have been notified to the Editor before submitting the Article for Double-Blind Review.

Responsibilities of the Authors

Authors must guarantee that their articles are the product of their original work and that the data has been obtained ethically.

Authors must ensure that they have not been previously published or that they are not considered in another serial publication.

Authors must strictly follow the rules for the publication of Defined Articles by the Editorial Board.

The authors have requested that the text in all its forms be an unethical editorial behavior and is unacceptable, consequently, any manuscript that incurs in plagiarism is eliminated and not considered for publication.

Authors should cite publications that have been influential in the nature of the Article submitted to arbitration.

Information services

Indexation - Bases and Repositories

LATINDEX (Scientific Journals of Latin America, Spain and Portugal)
RESEARCH GATE (Germany)
GOOGLE SCHOLAR (Citation indices-Google)
REDIB (Ibero-American Network of Innovation and Scientific Knowledge- CSIC)
MENDELEY (Bibliographic References Manager)

Publishing Services

Citation and Index Identification H
Management of Originality Format and Authorization
Testing Article with PLAGSCAN
Article Evaluation
Certificate of Double-Blind Review
Article Edition
Web layout
Indexing and Repository
ArticleTranslation
Article Publication
Certificate of Article
Service Billing

Editorial Policy and Management

21 Santa Lucía, CP-5220. Libertadores -Sucre–Bolivia. Phones: +52 1 55 6159 2296, +52 1 55 1260 0355, +52 1 55 6034 9181; Email: contact@ecorfan.org www.ecorfan.org

ECORFAN Journal-Bolivia

2410 4191
ISSN 2410-4191